

FUNCTIONAL A POSTERIORI ERROR ESTIMATES FOR BOUNDARY ELEMENT METHODS

STEFAN KURZ, DIRK PAULY, DIRK PRAETORIUS, SERGEY REPIN,
AND DANIEL SEBASTIAN

ABSTRACT. Functional error estimates are well-established tools for *a posteriori* error estimation and related adaptive mesh-refinement for the finite element method (FEM). The present work proposes a first functional error estimate for the boundary element method (BEM). One key feature is that the derived error estimates are independent of the BEM discretization and provide guaranteed lower and upper bounds for the unknown error. In particular, our analysis covers Galerkin BEM as well as collocation, which makes our approach of particular interest for people working in engineering. Numerical experiments for the Laplace problem confirm the theoretical results.

1. INTRODUCTION

Let $\Omega \subset \mathbb{R}^d$, $d \geq 2$, be a bounded Lipschitz domain with polygonal boundary $\Gamma := \partial\Omega$. We consider the Poisson problem with inhomogeneous Dirichlet boundary data g , i.e.,

$$\Delta u = 0 \quad \text{in } \Omega, \quad u = g \quad \text{on } \Gamma. \quad (1)$$

Throughout the paper, we assume that $d \in \{2, 3\}$. However, all results can easily be extended to higher dimensions. In case of $d = 2$, we suppose that $\text{diam}(\Omega) < 1$, which can always be achieved by scaling. For the numerical solution of (1), we employ the boundary element method (BEM); see, e.g., [Ste08a, SS11, GS18]. For the ease of presentation, let us consider an indirect ansatz based on the single-layer potential

$$(\tilde{V}\phi)(x) := \int_{\Gamma} G(x - y) \phi(y) dy = u(x) \quad \text{for all } x \in \Omega \quad (2)$$

with unknown integral density ϕ , where $G(z) = -\frac{1}{2\pi} \log |z|$ for $d = 2$ resp. $G(z) = \frac{1}{4\pi} |z|^{-1}$ for $d = 3$ denotes the fundamental solution of the Laplacian. Taking the trace on Γ , the potential ansatz leads to the weakly-singular integral equation

$$(V\phi)(x) = g(x) \quad \text{for almost all } x \in \Gamma, \quad (3)$$

where the integral representation of $g = V\phi$ coincides with that of $u = \tilde{V}\phi$ (at least for bounded densities) but is now evaluated on Γ (instead of inside Ω). Given a triangulation

2010 *Mathematics Subject Classification.* 65N38, 65N15, 65N50.

Key words and phrases. boundary element method, functional a posteriori error estimate, adaptive mesh-refinement.

Acknowledgement. D. Sebastian and D. Praetorius thankfully acknowledge support by the Austrian Science Fund (FWF) through the SFB *Taming complexity in partial differential systems*, and the stand-alone project *Optimal adaptivity for BEM and FEM-BEM coupling* (grant P27005). The work of S. Kurz was supported in part by the Excellence Initiative of the German Federal and State Governments, and in part by the *Graduate School of Computational Engineering* at TU Darmstadt.

\mathcal{F}_h^Γ of the boundary Γ , the latter equation is solved by the lowest-order BEM and provides some piecewise constant approximation ϕ_h , i.e.,

$$\phi \approx \phi_h \in \mathcal{P}^0(\mathcal{F}_h^\Gamma), \quad (4)$$

where the precise discretization (e.g., Galerkin BEM, collocation, etc.) will not be exploited by our analysis. However, as a BEM inherent characteristics, we obtain an approximation of the potential $u \approx u_h := \tilde{V}\phi_h$, which satisfies the Laplace problem $\Delta u_h = 0$ in Ω . The latter is the key argument for the error identity

$$\max_{\substack{\boldsymbol{\tau} \in \mathbf{L}^2(\Omega) \\ \operatorname{div} \boldsymbol{\tau} = 0}} \left(2 \langle g - u_h|_\Gamma, \mathbf{n} \cdot \boldsymbol{\tau}|_\Gamma \rangle_\Gamma - \|\boldsymbol{\tau}\|_{\mathbf{L}^2(\Omega)}^2 \right) = \|\nabla(u - u_h)\|_{\mathbf{L}^2(\Omega)}^2 = \min_{\substack{w \in \mathbf{H}^1(\Omega) \\ w|_\Gamma = g - u_h|_\Gamma}} \|\nabla w\|_{\mathbf{L}^2(\Omega)}^2, \quad (5)$$

where $\langle \cdot, \cdot \rangle_\Gamma$ denotes the extended $\mathbf{L}^2(\Gamma)$ scalar product (see Theorem 3 below). The identities (5) generate *a posteriori error estimates of the functional type* that are independent of the discretization and provide fully guaranteed lower and upper bounds for the unknown error without any constants at all. In general, these functional type a posteriori estimates involve only constants in basic functional inequalities associated with the concrete problem (e.g., Poincaré–Friedrichs type or trace inequalities) and are applicable for *any* approximation from the admissible energy class (see [Rep00, AP19] or the monograph [Rep08] and the references cited therein). In particular, the equations (5) have also been used in [Rep08] for the analysis of errors arising in the Trefftz method.

From (5), constant-free (i.e., with known constant 1) lower and upper bounds for the unknown *potential error* $\|\nabla(u - u_h)\|_{\mathbf{L}^2(\Omega)}$ can be obtained by choosing *arbitrary* instances of $\boldsymbol{\tau}$ and w . In the present work, we compute these bounds by solving problems in a suitable boundary layer $S \subset \Omega$ along Γ by use of the finite element method (FEM). Moreover, these bounds are then employed to drive an adaptive mesh-refinement for the triangulation \mathcal{F}_h^Γ of Γ and, as novelty, also quantify the accuracy $\|\nabla(u - u_h)\|_{\mathbf{L}^2(\Omega)}$ of the BEM induced potential $u_h = \tilde{V}\phi_h$ in each step of the adaptive algorithm. In particular, the latter quantification is essentially constant-free (up to data oscillations terms arising for the FEM majorant) and can thus also be used as reasonable stopping criterion for adaptive BEM computations. Especially for practical applications, this is an important step forward, since there exist neither *a posteriori* error estimates with constant 1 nor estimates for physically relevant errors. While available results focus on the density ϕ_h (see, e.g., [CS95, Car97, MSW98, CMS01, EH06, FLP08] for some prominent results or the surveys [CF01, FFH⁺15] and the references therein), estimating rather the energy error of u_h circumvents, in particular, BEM-natural challenges like the localization of non-integer Sobolev norms.

Outline. The remainder of this work is organized as follows: In Section 2, we collect the necessary notations as well as the fundamental properties of (Galerkin) BEM. In Section 3, we formulate our approach for functional *a posteriori* error estimation. Theorem 3 states the error identity (5). Theorem 4 provides a computable upper bound on (5) by means of an \mathbf{H}^1 -conforming FEM approach as well as a computable lower bound on (5) by means of an $\mathbf{H}(\operatorname{div})$ -conforming mixed FEM approach. Section 4 shows how these findings can be used to steer an adaptive mesh-refinement. Algorithm 9 formulates such a strategy with reliable error control on $\|\nabla(u - u_h)\|_{\mathbf{L}^2(\Omega)}$. In Section 5, we employ the

proposed adaptive algorithm to underpin our theoretical findings by some numerical experiments in 2D. Section 6 concludes the work with possible extensions of our analysis like higher-order BEM, alternative BEM discretizations like collocation, direct BEM formulations, and error control for exterior domain problems (where Ω is unbounded). The final Section 7 summarizes the contributions of the present work and addresses possible topics for future research.

2. PRELIMINARIES AND NOTATION

2.1. Domains and function spaces. Throughout this paper, let $\Omega \subset \mathbb{R}^d$, $d \in \{2, 3\}$, be a bounded Lipschitz domain (i.e., locally below the graph of some Lipschitz function) with boundary $\Gamma = \partial\Omega$ and normal vector field \mathbf{n} . For all numerical results involving discretisations, we assume that Γ is a polygon. We denote by $\langle \cdot, \cdot \rangle_{L^2(\Xi)}$ and $\|\cdot\|_{L^2(\Xi)}$ the standard inner product and norm in $L^2(\Xi)$, respectively, where, e.g., $\Xi \in \{\Omega, \Gamma\}$. Based on $L^2(\Omega)$, we define the Hilbert spaces

$$\begin{aligned} H^1(\Omega) &:= \{\varphi \in L^2(\Omega) : \nabla \varphi \in L^2(\Omega)\}, \\ H(\operatorname{div}, \Omega) &:= \{\boldsymbol{\sigma} \in L^2(\Omega) : \operatorname{div} \boldsymbol{\sigma} \in L^2(\Omega)\}. \end{aligned}$$

The corresponding inner products and (induced) norms are $\langle \cdot, \cdot \rangle_{H^1(\Omega)}$ and $\|\cdot\|_{H^1(\Omega)}$ resp. $\langle \cdot, \cdot \rangle_{H(\operatorname{div}, \Omega)}$ and $\|\cdot\|_{H(\operatorname{div}, \Omega)}$. Moreover, introducing the scalar trace operator $(\cdot)|_\Gamma : H^1(\Omega) \rightarrow L^2(\Gamma)$ together with its range $H^{1/2}(\Gamma)$ and equipped with the natural quotient norm, our analysis also employs

$$H_0^1(\Omega) := \{\varphi \in H^1(\Omega) : \varphi|_\Gamma = 0\},$$

which is a closed subspace of $H^1(\Omega)$. With the help of an extension operator $\widehat{(\cdot)} : H^{1/2}(\Gamma) \rightarrow H^1(\Omega)$, which comes together with the trace operator as a right inverse, we can construct a (unique) harmonic extension $\widehat{f} \in H^1(\Omega)$ of $f \in H^{1/2}(\Gamma)$ satisfying $\|\nabla \widehat{f}\|_{L^2(\Omega)} \leq \|f\|_{H^{1/2}(\Gamma)}$ and

$$\begin{aligned} \Delta \widehat{f} &= 0 \quad \text{in } \Omega, \\ \widehat{f}|_\Gamma &= f \quad \text{on } \Gamma. \end{aligned} \tag{6}$$

Finally, we need the dual space $H^{-1/2}(\Gamma) := H^{1/2}(\Gamma)'$ equipped with the natural norm

$$\|f\|_{H^{-1/2}(\Gamma)} := \sup_{0 \neq \psi \in H^{1/2}(\Gamma)} \frac{\langle \psi, f \rangle_\Gamma}{\|\psi\|_{H^{1/2}(\Gamma)}},$$

where the $H^{1/2}(\Gamma) \times H^{-1/2}(\Gamma)$ -duality product $\langle \cdot, \cdot \rangle_\Gamma$ extends, as usual, the $L^2(\Gamma)$ scalar product $\langle \cdot, \cdot \rangle_{L^2(\Gamma)}$. We recall that $H^{1/2}(\Gamma) \subset L^2(\Gamma) \subset H^{-1/2}(\Gamma)$ is a Gelfand triple and refer to [BBF13] for the fact that $H^{-1/2}(\Gamma)$ can also be characterised as the range of normal traces $\mathbf{n} \cdot (\cdot)|_\Gamma : H(\operatorname{div}, \Omega) \rightarrow H^{-1/2}(\Gamma)$ of $H(\operatorname{div}, \Omega)$ -vector fields, i.e.,

$$H^{-1/2}(\Gamma) = \{\mathbf{n} \cdot \boldsymbol{\sigma}|_\Gamma : \boldsymbol{\sigma} \in H(\operatorname{div}, \Omega)\}.$$

Definition 1. A subset $S \subset \Omega$ is called a boundary layer, if it is a Lipschitz domain with $\Gamma \subset \partial S$, which admits a conforming triangulation \mathcal{T}_h^S into simplices. We then define

$\Gamma^c := \partial S \setminus \Gamma$. In particular, we define the corresponding induced triangulation of Γ by

$$\mathcal{F}_h^\Gamma := \mathcal{T}_h^S|_\Gamma := \{F : F \subset \Gamma \text{ and } F \text{ is a face of some simplex } T \in \mathcal{T}_h^S\}. \quad (7)$$

For $q \in \mathbb{N}_0$ and \mathcal{P}^q being the space of polynomials of degree q , we define

$$\begin{aligned} \mathcal{P}^q(\mathcal{T}_h^S) &:= \{\varphi_h \in \mathbf{L}^\infty(S) : \varphi_h|_T \in \mathcal{P}^q \text{ for all } T \in \mathcal{T}_h^S\}, \\ \mathcal{P}^q(\mathcal{F}_h^\Gamma) &:= \{\psi_h \in \mathbf{L}^\infty(\Gamma) : \psi_h|_F \in \mathcal{P}^q \text{ for all } F \in \mathcal{F}_h^\Gamma\}. \end{aligned}$$

Moreover, for $p \in \mathbb{N}$, we employ the standard \mathbf{H}^1 -conforming FEM spaces

$$\begin{aligned} \mathcal{S}^p(\mathcal{T}_h^S) &:= \{\varphi_h \in \mathbf{C}^0(\overline{S}) : \varphi_h|_T \in \mathcal{P}^p \text{ for all } T \in \mathcal{T}_h^S\} \subset \mathbf{H}^1(S), \\ \mathcal{S}_0^p(\mathcal{T}_h^S) &:= \{\varphi_h \in \mathcal{S}^p(\mathcal{T}_h^S) : \varphi_h|_{\partial S} = 0\} \subset \mathbf{H}_0^1(S), \\ \mathcal{S}_{\Gamma^c}^p(\mathcal{T}_h^S) &:= \{\varphi_h \in \mathcal{S}^p(\mathcal{T}_h^S) : \varphi_h|_{\Gamma^c} = 0\}. \end{aligned}$$

Let \mathcal{F}_h^S denote the set of all interior faces, i.e., all $F \in \mathcal{F}_h^S$ admit unique $T_+, T_- \in \mathcal{T}_h^S$ with $F = T_+ \cap T_-$. For $q \in \mathbb{N}_0$, we define the $\mathbf{H}(\text{div})$ -conforming Raviart–Thomas space

$$\begin{aligned} \mathbf{RT}^q(\mathcal{T}_h^S) &= \{\boldsymbol{\sigma}_h \in \mathbf{L}^\infty(S) : \forall T \in \mathcal{T}_h^S \quad \exists (\mathbf{a}, b) \in \mathcal{P}^q(\mathbb{R}^d)^d \times \mathcal{P}^q(\mathbb{R}^d) \quad \forall x \in T \\ &\quad \boldsymbol{\sigma}_h(x) = \mathbf{a}(x) + b(x)x \quad \text{and} \quad \forall F \in \mathcal{F}_h^S \quad \mathbf{n}_F \cdot [\boldsymbol{\sigma}_h]_F = 0\} \subset \mathbf{H}(\text{div}, S), \end{aligned}$$

where \mathbf{n}_F is a normal vector for the face $F \in \mathcal{F}_h^S$ and $[\boldsymbol{\sigma}_h]_F := \boldsymbol{\sigma}_h|_{T_+} - \boldsymbol{\sigma}_h|_{T_-}$ denotes the jump of $\boldsymbol{\sigma}_h$ across F . Based on that, we let

$$\mathbf{RT}_{\Gamma^c}^q(\mathcal{T}_h^S) := \{\boldsymbol{\sigma}_h \in \mathbf{RT}^q(\mathcal{T}_h^S) : \mathbf{n} \cdot \boldsymbol{\sigma}_h|_{\Gamma^c} = 0\}.$$

Remark 2. In the proofs of Section 3 below, we exploit that for arbitrary $v_h \in \mathcal{S}_{\Gamma^c}^p(\mathcal{T}_h^S)$ and $\boldsymbol{\sigma}_h \in \mathbf{RT}_{\Gamma^c}^q(\mathcal{T}_h^S)$ the definitions

$$\check{v}_h := \begin{cases} v_h & \text{in } S \\ 0 & \text{in } \Omega \setminus S \end{cases} \quad \text{and} \quad \check{\boldsymbol{\sigma}}_h := \begin{cases} \boldsymbol{\sigma}_h & \text{in } S \\ 0 & \text{in } \Omega \setminus S \end{cases} \quad (8)$$

provide conforming extensions $\check{v}_h \in \mathbf{H}^1(\Omega)$ and $\check{\boldsymbol{\sigma}}_h \in \mathbf{H}(\text{div}, \Omega)$. In particular, we will implicitly identify v_h (resp. $\boldsymbol{\sigma}_h$) with its zero-extension \check{v}_h (resp. $\check{\boldsymbol{\sigma}}_h$).

2.2. General problem setting. From now on, we assume that Ω , Γ , and a boundary layer S together with Γ^c and corresponding FEM spaces are given. Let $g \in \mathbf{H}^{1/2}(\Gamma)$ and let $u \in \mathbf{H}^1(\Omega)$ be the unique solution of the homogeneous Dirichlet–Laplace problem

$$\Delta u = 0 \quad \text{in } \Omega, \quad (9a)$$

$$u = g \quad \text{on } \Gamma. \quad (9b)$$

In particular, we have $\nabla u \in \mathbf{H}(\text{div}, \Omega)$ with $\text{div } \nabla u = 0$. Note that $u = \widehat{g} \in \mathbf{H}^1(\Omega)$ is the unique harmonic extension of g with $\|\nabla u\|_{\mathbf{L}^2(\Omega)} \leq \|g\|_{\mathbf{H}^{1/2}(\Gamma)}$; see (6).

2.3. Weakly-singular integral equation. The single-layer potential (2) provides a continuous linear operator $\tilde{V} : H^{-1/2}(\Gamma) \rightarrow H^1(\Omega)$. Moreover, its concatenation with the trace defines a continuous linear operator $V : H^{-1/2}(\Gamma) \rightarrow H^{1/2}(\Gamma)$, which is elliptic on $H^{-1/2}(\Gamma)$ (under the scaling condition $\text{diam}(\Omega) < 1$ for $d = 2$). Hence, the Lax–Milgram lemma guarantees existence and uniqueness of $\phi \in H^{-1/2}(\Gamma)$ such that

$$\langle V\phi, \psi \rangle_\Gamma = \langle g, \psi \rangle_\Gamma \quad \text{for all } \psi \in H^{-1/2}(\Gamma). \quad (10)$$

According to the Hahn–Banach theorem, the latter variational formulation is equivalent to the identity $V\phi = g$ in $H^{1/2}(\Gamma)$ from (3). For details on elliptic boundary integral equations, we refer, e.g., to the monographs [McL00, HW08].

2.4. Galerkin boundary element method. Given a triangulation \mathcal{F}_h^Γ of Γ , the lowest-order Galerkin BEM seeks $\phi_h \in \mathcal{P}^0(\mathcal{F}_h^\Gamma)$, which solves the discretized weak form

$$\langle V\phi_h, \psi_h \rangle_{L^2(\Gamma)} = \langle g, \psi_h \rangle_{L^2(\Gamma)} \quad \text{for all } \psi_h \in \mathcal{P}^0(\mathcal{F}_h^\Gamma). \quad (11)$$

The Lax–Milgram lemma also applies to the conforming Galerkin discretization and proves existence and uniqueness of $\phi_h \in \mathcal{P}^0(\mathcal{F}_h^\Gamma)$. We note that in the discrete version (11) of (10) the $H^{1/2}(\Gamma) \times H^{-1/2}(\Gamma)$ duality product coincides, in fact, with the $L^2(\Gamma)$ scalar product. For details on the (Galerkin) boundary element method, we refer, e.g., to the monographs [Ste08a, SS11, GS18].

3. FUNCTIONAL A POSTERIORI BEM ERROR ESTIMATION

In this section, we prove the error identity (5) and provide efficiently computable upper and lower bounds for the potential error $\|\nabla(u - u_h)\|_{L^2(\Omega)}$, where $u \in H^1(\Omega)$ solves (9) and $u_h := \tilde{V}\phi_h$ is defined in (2).

3.1. Functional error identity. The fact that the error $u - u_h$ satisfies (9a) exactly is a powerful tool. However, the consideration of the potential u_h from a BEM comes with a drawback: it is not a discrete function and lacks further *a priori* knowledge like the Galerkin orthogonality, which is obviously never available for any approximation $u_h := \tilde{V}\phi_h \approx u \in H^1(\Omega)$. Functional *a posteriori* error estimates are eminently suitable for the BEM, since they do not require any such *a priori* assumption. On top of that, for homogeneous problems, they provide *constant-free* error identities by means of so-called primal and dual problems. For the Laplacian, the key argument is the Dirichlet principle:

Harmonic functions are minimisers of the Dirichlet energy $\|\nabla w\|_{L^2(\Omega)}^2$.

Note that the boundary residual $g - u_h|_\Gamma \in H^{1/2}(\Gamma)$ is essential for both the majorant $\overline{\mathfrak{M}}$ and the minorant $\underline{\mathfrak{M}}$, and comprises all relevant information about the error.

Theorem 3 (Functional *a posteriori* error identities). *For any approximation $v \in H^1(\Omega)$ with $\Delta v = 0$, the equalities (5) hold true. More precisely,*

$$\max_{\substack{\boldsymbol{\tau} \in L^2(\Omega) \\ \text{div } \boldsymbol{\tau} = 0}} \underline{\mathfrak{M}}(\boldsymbol{\tau}; v|_\Gamma, g) = \|\nabla(u - v)\|_{L^2(\Omega)}^2 = \min_{\substack{w \in H^1(\Omega) \\ w|_\Gamma = g - v|_\Gamma}} \overline{\mathfrak{M}}(\nabla w), \quad (12a)$$

where

$$\underline{\mathfrak{M}}(\boldsymbol{\tau}; v|_{\Gamma}, g) := 2 \langle g - v|_{\Gamma}, \boldsymbol{n} \cdot \boldsymbol{\tau}|_{\Gamma} \rangle_{\Gamma} - \|\boldsymbol{\tau}\|_{\mathbf{L}^2(\Omega)}^2, \quad \overline{\mathfrak{M}}(\nabla w) := \|\nabla w\|_{\mathbf{L}^2(\Omega)}^2. \quad (12b)$$

The unique maximiser is $\boldsymbol{\tau} = \nabla(u - v)$. The unique minimiser is $\bar{w} = u - v$.

Proof. The proof is split into two parts.

• **Upper bound:** Let $\tilde{w} \in H^1(\Omega)$ with $\tilde{w}|_{\Gamma} = u|_{\Gamma} = g$. Since we have $\Delta(u - v) = 0$ and $u - \tilde{w} \in H_0^1(\Omega)$, integration by parts shows that

$$\|\nabla(u - v)\|_{\mathbf{L}^2(\Omega)}^2 = \underbrace{\langle \nabla(u - \tilde{w}), \nabla(u - v) \rangle_{\mathbf{L}^2(\Omega)}}_{=0} + \langle \nabla(\tilde{w} - v), \nabla(u - v) \rangle_{\mathbf{L}^2(\Omega)}.$$

This yields $\|\nabla(u - v)\|_{\mathbf{L}^2(\Omega)} \leq \|\nabla(\tilde{w} - v)\|_{\mathbf{L}^2(\Omega)}$. The substitution $w := \tilde{w} - v$ proves that

$$\|\nabla(u - v)\|_{\mathbf{L}^2(\Omega)} \leq \inf_{\substack{w \in H^1(\Omega) \\ w|_{\Gamma} = g - v|_{\Gamma}}} \|\nabla w\|_{\mathbf{L}^2(\Omega)}.$$

The unique infimum is attained at $w = u - v$.

• **Lower bound:** In any Hilbert space \mathcal{H} , it holds that

$$\|a\|_{\mathcal{H}}^2 = \max_{b \in \mathcal{H}} (2 \langle a, b \rangle_{\mathcal{H}} - \|b\|_{\mathcal{H}}^2) \quad \text{for all } a \in \mathcal{H},$$

where the maximum is unique and attained for $b = a$. Since

$$\nabla(u - v) \in \mathcal{H} := \{\boldsymbol{\sigma} \in \mathbf{H}(\text{div}, \Omega) : \text{div } \boldsymbol{\sigma} = 0\},$$

we have

$$\begin{aligned} \|\nabla(u - v)\|_{\mathbf{L}^2(\Omega)}^2 &= \|\nabla(u - v)\|_{\mathcal{H}}^2 = \max_{\substack{\boldsymbol{\tau} \in \mathbf{L}^2(\Omega) \\ \text{div } \boldsymbol{\tau} = 0}} \left(2 \langle \nabla(u - v), \boldsymbol{\tau} \rangle_{\mathbf{L}^2(\Omega)} - \|\boldsymbol{\tau}\|_{\mathbf{L}^2(\Omega)}^2 \right) \\ &= \max_{\substack{\boldsymbol{\tau} \in \mathbf{L}^2(\Omega) \\ \text{div } \boldsymbol{\tau} = 0}} \left(2 \langle g - v|_{\Gamma}, \boldsymbol{n} \cdot \boldsymbol{\tau}|_{\Gamma} \rangle_{\Gamma} - \|\boldsymbol{\tau}\|_{\mathbf{L}^2(\Omega)}^2 \right). \end{aligned}$$

In particular, the maximum is attained for $\boldsymbol{\tau} = \nabla(u - v)$. This concludes the proof. \square

To ease the readability, the remainder of this chapter focusses on our numerical setup. For the functional analytic framework in a Sobolev space setting, which might be of independent interest, we refer to Appendix A below.

3.2. Computable error bounds. We aim at error bounds obtained by solving FEM problems on a boundary layer $S \subset \Omega$. For the maximization problem in (12), the constraint $\text{div } \boldsymbol{\tau} = 0$ can be realized by a mixed formulation (see also Lemma 15 in Appendix A). However, the boundary condition $w|_{\Gamma} = g - v|_{\Gamma}$ cannot be satisfied exactly by any piecewise polynomial solution w_h corresponding to (12). Therefore, the upper bound involves an additional oscillation term given by a discretisation operator J_h .

Theorem 4 (Computable bounds via boundary layer). *Let $v \in H^1(\Omega)$ with $\Delta v = 0$. Let $p \in \mathbb{N}$ and $J_h : H^{1/2}(\Gamma) \rightarrow \mathcal{S}^p(\mathcal{F}_h^{\Gamma}) := \{\varphi_h|_{\Gamma} : \varphi_h \in \mathcal{S}^p(\mathcal{T}_h^S)\}$. Moreover, let*

$w_h \in \mathcal{S}^p(\mathcal{T}_h^S)$ be the unique solution of

$$\langle \nabla w_h, \nabla \varphi_h \rangle_{\mathbf{L}^2(S)} = 0 \quad \text{for all } \varphi_h \in \mathcal{S}_0^p(\mathcal{T}_h^S) \quad \text{with } w_h|_{\partial S} = \begin{cases} J_h(g - v|_\Gamma) & \text{on } \Gamma, \\ 0 & \text{on } \Gamma^c. \end{cases} \quad (13)$$

For $q \in \mathbb{N}_0$, let the pair $(\boldsymbol{\tau}_h, \omega_h) \in \mathbf{RT}_{\Gamma^c}^q(\mathcal{T}_h^S) \times \mathcal{P}^q(\mathcal{T}_h^S)$ be the unique solution of

$$\langle \boldsymbol{\tau}_h, \boldsymbol{\sigma}_h \rangle_{\mathbf{L}^2(S)} + \langle \operatorname{div} \boldsymbol{\sigma}_h, \omega_h \rangle_{\mathbf{L}^2(S)} = \langle g - v|_\Gamma, \mathbf{n} \cdot \boldsymbol{\sigma}_h|_\Gamma \rangle_\Gamma \quad \text{for all } \boldsymbol{\sigma}_h \in \mathbf{RT}_{\Gamma^c}^q(\mathcal{T}_h^S), \quad (14a)$$

$$\langle \operatorname{div} \boldsymbol{\tau}_h, \psi_h \rangle_{\mathbf{L}^2(S)} = 0 \quad \text{for all } \psi_h \in \mathcal{P}^q(\mathcal{T}_h^S). \quad (14b)$$

Then, it holds that

$$2 \langle g - v|_\Gamma, \mathbf{n} \cdot \boldsymbol{\tau}_h|_\Gamma \rangle_{\mathbf{L}^2(\Gamma)} - \|\boldsymbol{\tau}_h\|_{\mathbf{L}^2(S)}^2 \leq \|\nabla(u - v)\|_{\mathbf{L}^2(\Omega)}^2 \quad (15)$$

$$\leq \|\nabla w_h\|_{\mathbf{L}^2(S)} + \|(1 - J_h)(g - v|_\Gamma)\|_{\mathbf{H}^{1/2}(\Gamma)}. \quad (16)$$

Proof. It is well-known that (13) admits a unique solution $w_h \in \mathcal{S}^p(\mathcal{T}_h^S)$, being the natural FEM discretization of an homogeneous Dirichlet–Laplace problem with inhomogeneous Dirichlet conditions; see, e.g., [BCD04, SV06, AFK⁺13]. To prove the upper bound (16), let $\widehat{f}_h \in \mathbf{H}^1(\Omega)$ be the (unique) harmonic extension of $f_h := (1 - J_h)(g - v|_\Gamma)$; see (6). Then, $\|\nabla \widehat{f}_h\|_{\mathbf{L}^2(\Omega)} \leq \|f_h\|_{\mathbf{H}^{1/2}(\Gamma)}$, and Theorem 3 leads to

$$\begin{aligned} \|\nabla(u - v)\|_{\mathbf{L}^2(\Omega)} &= \min_{\substack{w \in \mathbf{H}^1(\Omega) \\ w|_\Gamma = g - v|_\Gamma}} \|\nabla w\|_{\mathbf{L}^2(\Omega)} \leq \min_{\substack{w \in \mathbf{H}^1(\Omega) \\ w|_\Gamma = g - v|_\Gamma}} \|\nabla(w - \widehat{f}_h)\|_{\mathbf{L}^2(\Omega)} + \|\nabla \widehat{f}_h\|_{\mathbf{L}^2(\Omega)} \\ &= \min_{\substack{w \in \mathbf{H}^1(\Omega) \\ w|_\Gamma = J_h(g - v|_\Gamma)}} \|\nabla w\|_{\mathbf{L}^2(\Omega)} + \|\nabla \widehat{f}_h\|_{\mathbf{L}^2(\Omega)}. \end{aligned}$$

Since the zero-extension of w_h belongs to $\mathbf{H}^1(\Omega)$ according to Remark 2, this proves that

$$\begin{aligned} \|\nabla(u - v)\|_{\mathbf{L}^2(\Omega)} &\leq \min_{\substack{w \in \mathbf{H}^1(\Omega) \\ w|_\Gamma = J_h(g - v|_\Gamma)}} \|\nabla w\|_{\mathbf{L}^2(\Omega)} + \|(1 - J_h)(g - v|_\Gamma)\|_{\mathbf{H}^{1/2}(\Gamma)} \\ &\leq \|\nabla w_h\|_{\mathbf{L}^2(S)} + \|(1 - J_h)(g - v|_\Gamma)\|_{\mathbf{H}^{1/2}(\Gamma)} \end{aligned}$$

and hence verifies the computable upper bound (16).

For existence and uniqueness of (14), we refer, e.g., to [BBF13, BC05]. Since $\operatorname{div} \boldsymbol{\tau}_h \in \mathcal{P}^q(\mathcal{T}_h^S) \subset \mathbf{L}^2(\Omega)$ by definition of $\mathbf{RT}^q(\mathcal{T}_h^S)$, it follows from (14b) that $\boldsymbol{\tau}_h \in \mathbf{RT}_{\Gamma^c}^q(\mathcal{T}_h^S) \subset \mathbf{H}(\operatorname{div}, S)$ with $\operatorname{div} \boldsymbol{\tau}_h = 0$ in S . According to Remark 2, the zero-extension of $\boldsymbol{\tau}_h$ belongs to $\mathbf{H}(\operatorname{div}, \Omega)$ with $\operatorname{div} \boldsymbol{\tau}_h = 0$ in Ω . The computable lower bound (15) thus follows from Theorem 3. \square

In order to circumvent the implementation of the constraint $\operatorname{div} \boldsymbol{\tau} = 0$, it is also an option to reformulate the maximization problem in (12) by means of potentials. While the 3D case involves vector potentials, for 2D such an approach is particularly attractive due to the possible use of scalar potentials. In the following, we thus concentrate on $d = 2$ (and refer to Appendix A for $d = 3$).

To this end, we recall the definitions of the 2D curl operators

$$\mathbf{curl} \varphi = \begin{bmatrix} -\partial_2 \varphi \\ \partial_1 \varphi \end{bmatrix} \quad \text{for } \varphi : \Omega \rightarrow \mathbb{R} \quad \text{resp.} \quad \operatorname{curl} \boldsymbol{\varphi} = \partial_1 \varphi_2 - \partial_2 \varphi_1 \quad \text{for } \boldsymbol{\varphi} : \Omega \rightarrow \mathbb{R}^2.$$

Note that $\operatorname{div} \mathbf{curl} \varphi = 0$. For $\varphi \in \mathbf{H}^1(\Omega)$, we thus have $\mathbf{curl} \varphi \in \mathbf{H}(\operatorname{div}, \Omega)$ so that the Neumann trace

Corollary 5 (Computable lower bound via boundary layer — \mathbf{H}^1 -conforming). *Suppose that $d = 2$. Let $v \in \mathbf{H}^1(\Omega)$ with $\Delta v = 0$. For $p \in \mathbb{N}$, let $\tilde{w}_h \in \mathcal{S}_{\Gamma^c}^p(\mathcal{T}_h^S)$ be the unique solution of*

$$\langle \nabla \tilde{w}_h, \nabla \varphi_h \rangle_{\mathbf{L}^2(S)} = \langle g - v|_{\Gamma}, \mathbf{n} \cdot \mathbf{curl} \varphi_h|_{\Gamma} \rangle_{\Gamma} \quad \text{for all } \varphi_h \in \mathcal{S}_{\Gamma^c}^p(\mathcal{T}_h^S). \quad (17)$$

Then, it holds that

$$2\langle g - v|_{\Gamma}, \mathbf{n} \cdot \mathbf{curl} \tilde{w}_h|_{\Gamma} \rangle_{\Gamma} - \|\nabla \tilde{w}_h\|_{\mathbf{L}^2(S)}^2 \leq \|\nabla(u - v)\|_{\mathbf{L}^2(\Omega)}^2.$$

Proof. It is well-known that (17) admits a unique solution $\tilde{w}_h \in \mathcal{S}_{\Gamma^c}^p(\mathcal{T}_h^S)$ being the natural FEM discretization of a mixed Dirichlet–Neumann–Laplace problem; see, e.g., [BCD04]. According to Remark 2, the zero-extension of \tilde{w}_h belongs to $\mathbf{H}^1(\Omega)$ and hence $\tilde{\boldsymbol{\tau}}_h := \mathbf{curl} \tilde{w}_h \in \mathbf{H}(\operatorname{div}, \Omega)$ satisfies that $\operatorname{div} \tilde{\boldsymbol{\tau}}_h = 0$ with $\mathbf{n} \cdot \mathbf{curl} \tilde{w}_h|_{\Gamma} = \mathbf{n} \cdot \tilde{\boldsymbol{\tau}}_h|_{\Gamma}$ and $\|\tilde{\boldsymbol{\tau}}_h\|_{\mathbf{L}^2(\Omega)} = \|\mathbf{curl} \tilde{w}_h\|_{\mathbf{L}^2(\Omega)} = \|\nabla \tilde{w}_h\|_{\mathbf{L}^2(\Omega)}$. The claim thus follows from Theorem 3. \square

4. ADAPTIVE ALGORITHM

4.1. Triangulations and mesh-refinement. In our numerical experiments, we start from a conforming simplicial triangulation \mathcal{T}_h such that $\Gamma \subset \bigcup_{T \in \mathcal{T}_h} T \subseteq \bar{\Omega}$. We obtain the boundary layer $S \subset \Omega$ as the second-order patch of Γ with respect to \mathcal{T}_h , i.e.,

$$\mathcal{T}_h^S := \{T \in \mathcal{T}_h : \exists T' \in \mathcal{T}_h, \quad T' \cap \Gamma \neq \emptyset \neq T \cap T'\} \quad \text{and} \quad S := \operatorname{interior}\left(\bigcup_{T \in \mathcal{T}_h^S} T\right). \quad (18)$$

Moreover, recall the BEM mesh $\mathcal{F}_h^{\Gamma} := \mathcal{T}_h^S|_{\Gamma} = \mathcal{T}_h|_{\Gamma}$ from (7). These definitions are illustrated in Figure 1.

For (local) mesh-refinement, we employ newest vertex bisection; see, e.g., [Ste08b, KPP13]. The adaptive strategy will only mark elements of \mathcal{T}_h^S , but refinement will be done with respect to the full triangulation \mathcal{T}_h . In particular, we stress that the second-order patch S will generically change, if the triangulation \mathcal{T}_h is refined; see, e.g., Figure 2. In this way, we guarantee that the number of degrees of freedom with respect to \mathcal{T}_h^S will increase proportionally to those with respect to \mathcal{F}_h^{Γ} ; see also Tables 2–5 below.

4.2. Data oscillations. The upper bound (16) in Theorem 4 involves the data approximation term $\|(1 - J_h)(g - u_h|_{\Gamma})\|_{\mathbf{H}^{1/2}(\Gamma)}$, where $u_h := \tilde{V}\phi_h$. Besides the fact that we still have to specify the operator $J_h : \mathbf{H}^{1/2}(\Gamma) \rightarrow \mathcal{S}^p(\mathcal{F}_h^{\Gamma}) = \{\varphi_h|_{\Gamma} : \varphi_h \in \mathcal{S}^p(\mathcal{T}_h)\}$, we note that the nonlocal nature of the $\mathbf{H}^{1/2}(\Gamma)$ -norm makes this term hardly computable.

In the following, we choose $J_h : \mathbf{L}^2(\Gamma) \rightarrow \mathcal{S}^p(\mathcal{F}_h^{\Gamma})$ as the $\mathbf{L}^2(\Gamma)$ -orthogonal projection onto the FEM space $\mathcal{S}^p(\mathcal{F}_h^{\Gamma})$. For $d = 2$, it follows under mild conditions on \mathcal{F}_h^{Γ} that J_h is $\mathbf{H}^1(\Gamma)$ -stable, i.e.,

$$\|\nabla J_h f\|_{\mathbf{L}^2(\Gamma)} \leq C_{\text{stab}} \|\nabla f\|_{\mathbf{L}^2(\Gamma)} \quad \text{for all } f \in \mathbf{H}^1(\Gamma); \quad (19)$$

see [CT87]. We note that these conditions are automatically satisfied for $\mathcal{F}_h^{\Gamma} = \mathcal{T}_h|_{\Gamma}$, since \mathcal{T}_h is only refined by newest vertex bisection. For $d = 3$, the $\mathbf{H}^1(\Gamma)$ -stability (19) is

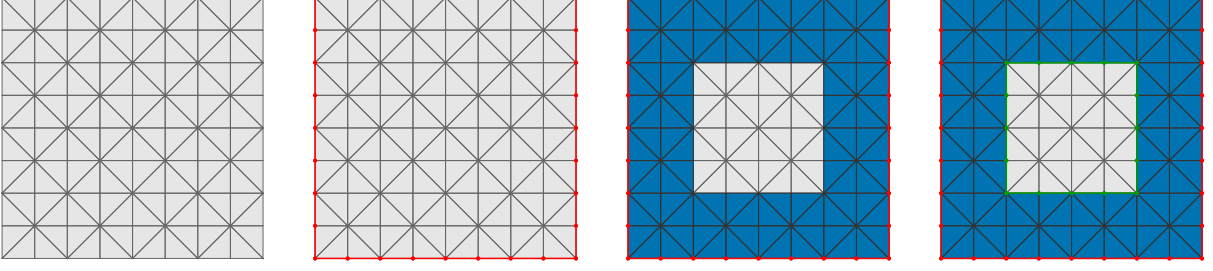


FIGURE 1. Example geometry $\Omega = (0, 1/2)^2$ with FEM triangulation \mathcal{T}_h (gray, left), induced BEM mesh \mathcal{F}_h^Γ on $\Gamma = \partial\Omega$ (red), generated boundary layer \mathcal{S} with mesh $\mathcal{T}_h^{\mathcal{S}}$ (blue), and interior boundary Γ^c (green), illustrated from left to right.

known for low-order FEM (on the 2D manifold Γ); see [KPP13] for $p = 1$ and [GHS16] for $p \in \{1, \dots, 12\}$. We recall the following result from [AFF⁺15]:

Lemma 6. *If the $\mathbf{L}^2(\Gamma)$ -orthogonal projection $J_h : \mathbf{L}^2(\Gamma) \rightarrow \mathcal{S}^p(\mathcal{F}_h^\Gamma)$ is $\mathbf{H}^1(\Gamma)$ -stable (19), then it holds for all $f \in \mathbf{H}^1(\Gamma)$ that*

$$C_{\text{osc}}^{-1} \|(1 - J_h)f\|_{\mathbf{H}^{1/2}(\Gamma)} \leq \min_{f_h \in \mathcal{S}^p(\mathcal{F}_h^\Gamma)} \|f - f_h\|_{\mathbf{H}^{1/2}(\Gamma)} \leq C_{\text{osc}} \min_{f_h \in \mathcal{S}^p(\mathcal{F}_h^\Gamma)} \|h^{1/2} \nabla_\Gamma(f - f_h)\|_{\mathbf{L}^2(\Gamma)},$$

where $h \in \mathbf{L}^\infty(\Omega)$ is the local mesh-width function defined by $h|_F := \text{diam}(F)$ for all $F \in \mathcal{F}_h^\Gamma$. The constant $C_{\text{osc}} > 0$ depends only on C_{stab} and the shape regularity of \mathcal{T}_h .

Provided that the given Dirichlet boundary data satisfy $g \in \mathbf{H}^1(\Gamma)$, the foregoing lemma allows to dominate the data approximation term by

$$C_{\text{osc}}^{-2} \|(1 - J_h)(g - u_h|_\Gamma)\|_{\mathbf{H}^{1/2}(\Gamma)} \leq \|h^{1/2} \nabla_\Gamma((1 - J_h)(g - u_h|_\Gamma))\|_{\mathbf{L}^2(\Gamma)} =: \text{osc}_h, \quad (20)$$

where osc_h is, in fact, computable, while the constant C_{osc} is generic and hardly accessible. With $v = u_h$, the upper bound (16) becomes

$$\begin{aligned} \|\nabla(u - u_h)\|_{\mathbf{L}^2(\Omega)} &\leq \|\nabla w_h\|_{\mathbf{L}^2(\mathcal{S})} + \|(1 - J_h)(g - u_h|_\Gamma)\|_{\mathbf{H}^{1/2}(\Gamma)} \\ &\leq \|\nabla w_h\|_{\mathbf{L}^2(\mathcal{S})} + C_{\text{osc}}^2 \text{osc}_h, \end{aligned} \quad (21)$$

where $w_h \in \mathcal{S}^p(\mathcal{T}_h^{\mathcal{S}})$ solves (13). For the use in the adaptive algorithm, we note that

$$\text{osc}_h^2 = \sum_{T \in \mathcal{T}_h^{\mathcal{S}}} \text{osc}_h(T)^2, \text{ where } \text{osc}_h(T)^2 := \sum_{\substack{F \in \mathcal{F}_h^\Gamma \\ F \subset T}} \text{diam}(F) \|\nabla_\Gamma((1 - J_h)(g - u_h|_\Gamma))\|_{\mathbf{L}^2(F)}^2. \quad (22)$$

Remark 7. *In our numerical experiments, we will consider $p = 1$ as well as $p = 2$ to compute the uppermost bound in (21). Since the lower bound (15) is independent of the data approximation, we did only implement the lowest-order case $q = 0$.*

Remark 8. *Instead of the $\mathbf{L}^2(\Gamma)$ -orthogonal projection, one can also employ the Scott–Zhang projector; see [AFK⁺13, FFK⁺14]. Then, Lemma 6 as well as (20) hold accordingly. For $d = 2$, one can also employ nodal projection. While generic $\mathbf{H}^{1/2}(\Gamma)$ functions do not have to be continuous and Lemma 6 fails, one can still prove (20); see [FPP14, FFK⁺14].*

4.3. Adaptive algorithm. We propose the following algorithm, which is empirically tested for 2D model problems below.

Algorithm 9. Let $p \in \mathbb{N}$ and let $0 < \theta \leq 1$ be a fixed marking parameter. Let \mathcal{T}_h be a conforming initial triangulation of Ω . Let $\varepsilon > 0$ be the tolerance for the energy error $\|\nabla(u - u_h)\|_{L^2(\Omega)}$ with $u_h = \tilde{V}\phi_h$. Then, perform the following steps (i) – (ix):

- (i) Extract the BEM triangulation $\mathcal{F}_h^\Gamma = \mathcal{T}_h|_\Gamma$ from (7).
- (ii) Extract the patch $S \subset \Omega$ of Γ and the corresponding triangulation \mathcal{T}_h^S from (18).
- (iii) Compute the BEM solution $\phi_h \in \mathcal{P}^0(\mathcal{F}_h^\Gamma)$ of (11).
- (iv) Compute $J_h(g - u_h|_\Gamma)$ together with its oscillations $\text{osc}_h(T)$ of (22) for all $T \in \mathcal{T}_h$.
- (v) Compute the FEM solution $w_h \in \mathcal{S}^p(\mathcal{T}_h^S)$ of (13) for the majorant (16).
- (vi) Compute the error indicators

$$\eta_h(T) = \begin{cases} \|\nabla w_h\|_{L^2(T)} & \text{for } T \in \mathcal{T}_h^S, \\ 0 & \text{for } T \in \mathcal{T}_h \setminus \mathcal{T}_h^S. \end{cases} \quad (23)$$

- (vii) If $\overline{\mathfrak{M}}(\nabla w_h) = \sum_{T \in \mathcal{T}_h^S} \eta_h(T)^2 \leq \varepsilon^2$, then **break**.
- (viii) Otherwise, determine a set $\mathcal{M}_h \subseteq \mathcal{T}_h^S$ of minimal cardinality such that

$$\theta \sum_{T \in \mathcal{T}_h^S} [\eta_h(T)^2 + \text{osc}_h(T)^2] \leq \sum_{T \in \mathcal{M}_h} [\eta_h(T)^2 + \text{osc}_h(T)^2]. \quad (24)$$

- (ix) Refine (at least) all $T \in \mathcal{M}_h \subseteq \mathcal{T}_h$ by newest vertex bisection to obtain a new triangulation \mathcal{T}_h .

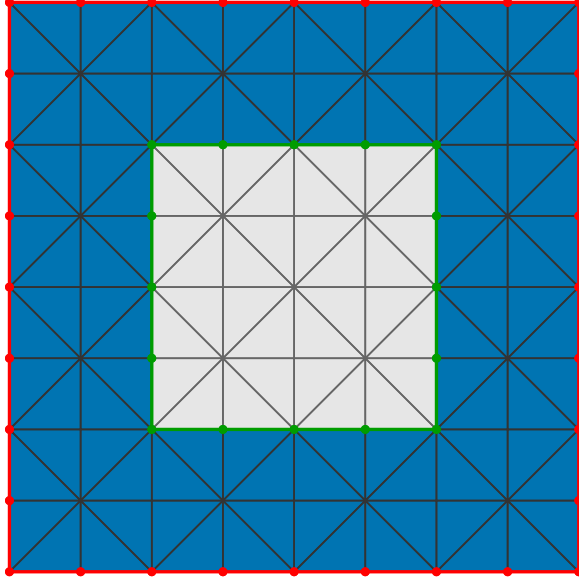
Remark 10. We note that a reliable adaptive algorithm mandatorily relies on a computable upper bound. Optionally, one can furthermore include the computation of a lower bound to provide a guaranteed confidence interval for the error: Computing the FEM solution $(\boldsymbol{\tau}_h, \phi_h) \in \text{RT}_{\Gamma^c}^0(\mathcal{T}_h^S) \times \mathcal{P}^0(\mathcal{T}_h^S)$ of (14), we can also assemble the discrete minorant

$$\underline{\mathfrak{M}}_h(\boldsymbol{\tau}_h; u_h|_\Gamma, g) = 2 \int_\Gamma (g - u_h|_\Gamma)(\mathbf{n} \cdot \boldsymbol{\tau}_h|_\Gamma) \, dx - \|\boldsymbol{\tau}_h\|_{L^2(S)}^2 \quad (25)$$

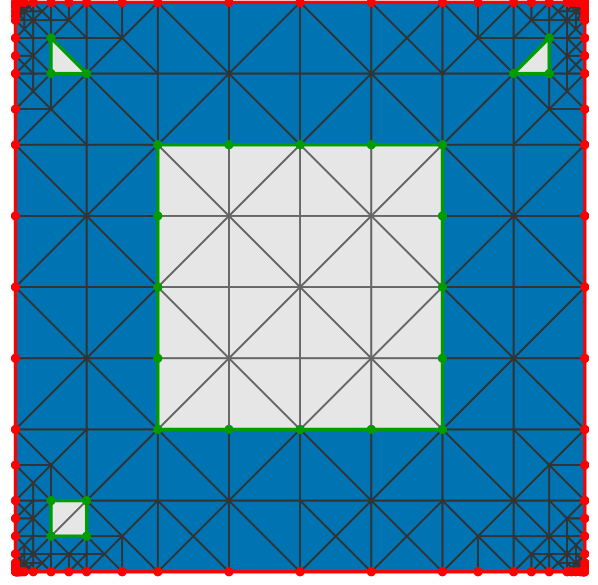
from Theorem 4. This is also done in the numerical experiments in Section 5. While $\underline{\mathfrak{M}}_h(\boldsymbol{\tau}_h; u_h|_\Gamma, g) \geq 0$ is not necessarily satisfied, this is empirically observed throughout all experiments below. Moreover, if one aims for sharper error bounds for a fixed approximate solution u_h , one can solve (13) and (14) (resp. (17)) by adaptive FEM on separate (generically) different boundary layers [Seb19].

5. NUMERICAL EXPERIMENTS

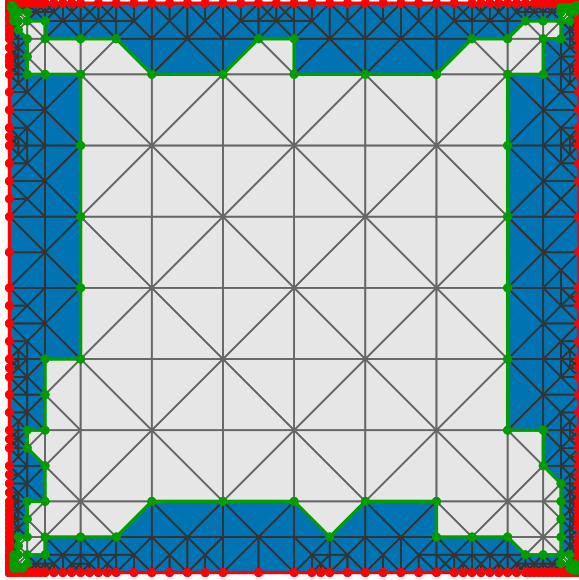
This section reports on some 2D numerical experiments to underline the accuracy of the introduced error estimates and the performance of the proposed adaptive strategy from Algorithm 9. All computations are done in MATLAB, where we build on the toolbox HILBERT from [AEF⁺14] for the lowest-order BEM, on [FPW11] for \mathcal{P}^1 -FEM (resp. [FFP19] for \mathcal{P}^2 -FEM), and on [BC05] for the lowest-order RT-FEM. Throughout, we consider Algorithm 9 for uniform mesh-refinement (i.e., $\theta = 1$) as well as for adaptive mesh-refinement (i.e., $0 < \theta < 1$).



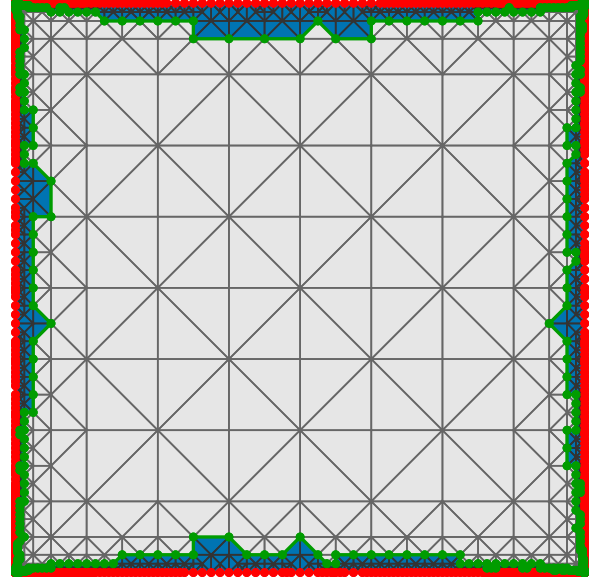
a) $\#\mathcal{T}_h^S = 72$, $\#\mathcal{F}_h^\Gamma = 32$, $\ell = 0$



b) $\#\mathcal{T}_h^S = 314$, $\#\mathcal{F}_h^\Gamma = 119$, $\ell = 17$



c) $\#\mathcal{T}_h^S = 923$, $\#\mathcal{F}_h^\Gamma = 352$, $\ell = 27$



d) $\#\mathcal{T}_h^S = 3176$, $\#\mathcal{F}_h^\Gamma = 1148$, $\ell = 38$

FIGURE 2. Adaptively generated meshes in Example 5.1 for $p = 1$ and $\theta = 0.6$. We indicate the boundary layer S (blue), the boundary Γ (red), and the interior boundary $\Gamma^c = \partial S \setminus \Gamma$ (green). The triangles $T \in \mathcal{T}_h^S \subset \mathcal{T}_h$ are indicated in blue. The triangles $T \in \mathcal{T}_h \setminus \mathcal{T}_h^S$ are indicated in gray.

Example 5.1 (Smooth potential in square domain). We consider problem (1) with prescribed exact solution

$$u(x) = \cosh(x_1) \cos(x_2) \quad \text{for all } x \in \Omega := (0, 1/2)^2 \quad (26)$$

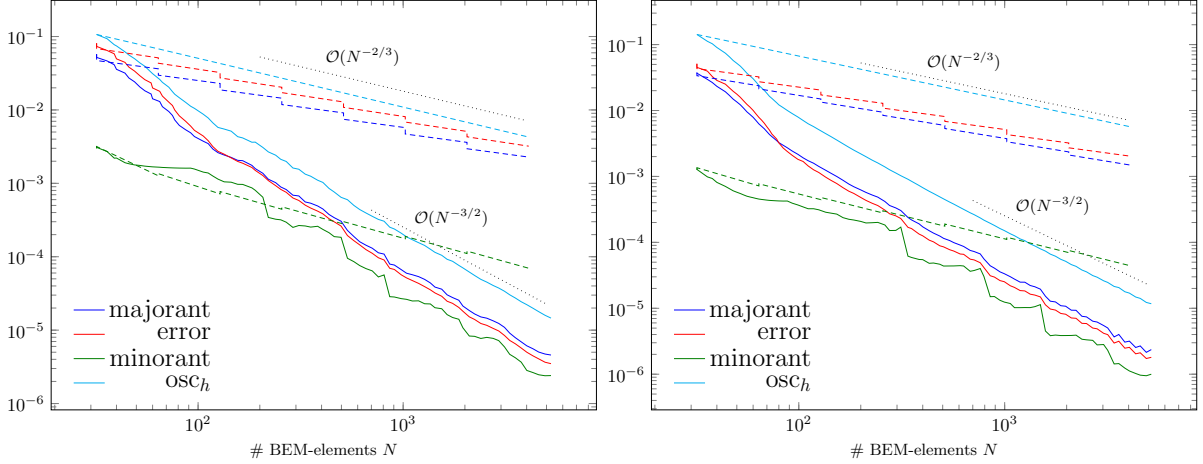


FIGURE 3. Comparison of adaptive mesh-refinement with $\theta = 0.4$ (solid) vs. uniform mesh-refinement (dashed) in Example 5.1. The majorant is computed by \mathcal{P}^1 -FEM (left) and \mathcal{P}^2 -FEM (right). We compare the potential error $\|\nabla(u - u_h)\|_{L^2(\Omega)}$, the majorant $\|\nabla w_h\|_{L^2(\Omega)}$ from (16), the data oscillations osc_h from (20), and the minorant $\underline{\mathfrak{M}}(\tau_h)^{1/2}$ from (25).

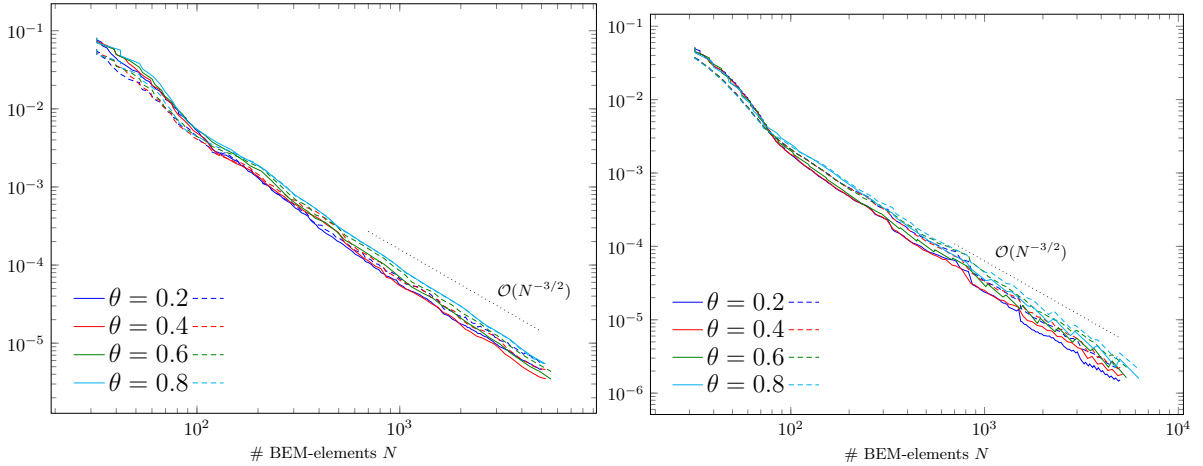


FIGURE 4. Influence of the marking parameter $\theta \in \{0.2, 0.4, 0.6, 0.8\}$ on adaptive mesh-refinement in Example 5.1. The majorant is computed by \mathcal{P}^1 -FEM (left) and \mathcal{P}^2 -FEM (right). We compare the potential error (solid) $\|\nabla(u - u_h)\|_{L^2(\Omega)}$ as well as the majorant (dashed) $\|\nabla w_h\|_{L^2(\Omega)}$ from (16).

on the square domain Ω with diameter $\text{diam}(\Omega) = \sqrt{1/2}$. We start Algorithm 9 with an initial triangulation \mathcal{T}_h of Ω into $\#\mathcal{T}_h = 128$ right triangles.

Even though u as well as its Dirichlet data $g = u|_{\Gamma}$ are smooth, we note that the sought integral density $\phi \in H^{-1/2}(\Gamma)$ of the indirect formulation (3) has no physical meaning and usually lacks smoothness (by inheriting the generic singularities from the interior as well as the exterior domain problem). Consequently, one may expect that uniform mesh-refinement (on the boundary) will not reveal the optimal convergence behavior

ℓ	$\#\mathcal{F}_h^\Gamma$	$\frac{\#\mathcal{T}_h^S}{\#\mathcal{F}_h^\Gamma}$	$\ \nabla(u - u_h)\ _{L^2(\Omega)}$	$\ \nabla w_h\ _{L^2(S)}$	$\frac{\ \nabla w_h\ _{L^2(S)}}{\ \nabla(u - u_h)\ _{L^2(\Omega)}}$	$\frac{\ \nabla w_h\ _{L^2(S)}}{\underline{\mathfrak{M}}(\tau_h)^{1/2}}$
0	32	2.25	$8.01e - 2$	$5.75e - 2$	0.71	19.16
1	64	2.63	$5.12e - 2$	$3.63e - 2$	0.71	28.67
2	128	2.81	$3.23e - 2$	$2.30e - 2$	0.71	31.96
3	256	2.91	$2.03e - 2$	$1.45e - 2$	0.71	32.56
4	512	2.95	$1.28e - 2$	$9.11e - 3$	0.71	32.66
5	1024	2.98	$8.08e - 3$	$5.74e - 3$	0.71	32.67
6	2048	2.99	$5.09e - 3$	$3.62e - 3$	0.71	32.67
7	4096	3.00	$3.21e - 3$	$2.28e - 3$	0.71	32.67

TABLE 1. Uniform mesh-refinement in Example 5.1. We focus on the degrees of freedom, the potential error $\|\nabla(u - u_h)\|_{L^2(\Omega)}$, the accuracy of the \mathcal{P}^1 -FEM majorant $\|\nabla w_h\|_{L^2(\Omega)}$ from (16), and the width of the confidence interval given by the quotient of majorant and minorant.

ℓ	$\#\mathcal{F}_h^\Gamma$	$\frac{\#\mathcal{T}_h^S}{\#\mathcal{F}_h^\Gamma}$	$\text{dof}(\mathcal{T}_h^S)$	$\ \nabla(u - u_h)\ _{L^2(\Omega)}$	$\ \nabla w_h\ _{L^2(S)}$	$\frac{\ \nabla w_h\ _{L^2(S)}}{\ \nabla(u - u_h)\ _{L^2(\Omega)}}$	$\frac{\ \nabla w_h\ _{L^2(S)}}{\underline{\mathfrak{M}}(\tau_h)^{1/2}}$
0	32	2.25	15	$8.01e - 2$	$5.75e - 2$	0.71	19.16
4	40	2.33	28	$4.97e - 2$	$3.58e - 2$	0.72	16.17
10	59	2.44	60	$2.33e - 2$	$1.65e - 2$	0.71	9.78
16	77	2.66	103	$9.95e - 3$	$7.29e - 3$	0.73	4.50
22	112	2.60	148	$3.81e - 3$	$3.48e - 3$	0.91	2.51
28	165	2.82	234	$1.88e - 3$	$2.03e - 3$	1.08	2.11
34	253	2.83	343	$8.27e - 4$	$8.92e - 4$	1.08	2.80
40	383	2.81	512	$4.18e - 4$	$4.91e - 4$	1.18	1.89
46	575	2.70	707	$1.66e - 4$	$1.89e - 4$	1.14	2.20
52	860	2.63	978	$6.96e - 5$	$7.94e - 5$	1.14	2.78
58	1072	2.61	1389	$3.92e - 5$	$4.92e - 5$	1.25	2.15
64	1869	2.61	2008	$2.04e - 5$	$2.55e - 5$	1.25	1.82
70	2748	2.58	2803	$1.06e - 5$	$1.34e - 5$	1.27	1.73
76	4007	2.55	3976	$5.00e - 6$	$6.12e - 6$	1.22	2.16
80	5259	2.53	5077	$3.50e - 6$	$4.58e - 6$	1.31	1.90

TABLE 2. Adaptive mesh-refinement with $\theta = 0.4$ in Example 5.1. We focus on the degrees of freedom, the potential error $\|\nabla(u - u_h)\|_{L^2(\Omega)}$, the accuracy of the \mathcal{P}^1 -FEM majorant $\|\nabla w_h\|_{L^2(\Omega)}$ from (16), and the width of the confidence interval given by the quotient of majorant and minorant.

$\|\phi - \phi_h\|_{H^{-1/2}(\Gamma)} = \mathcal{O}(h^{3/2}) = \mathcal{O}(N^{-3/2})$, where $N = \#\mathcal{F}_h^\Gamma$ is the number of elements of a uniform mesh \mathcal{F}_h^Γ of Γ and $3/2$ is the best possible convergence rate for a piecewise constant approximation $\phi \approx \phi_h \in \mathcal{P}^0(\mathcal{F}_h^\Gamma)$.

The initial meshes and some adaptively generated meshes are visualized in Figure 2. Figure 3 shows the resulting potential error and the computed minorant (15) and majorant (16), as well as the corresponding data oscillations (20) for $p = 1$ resp. $p = 2$.

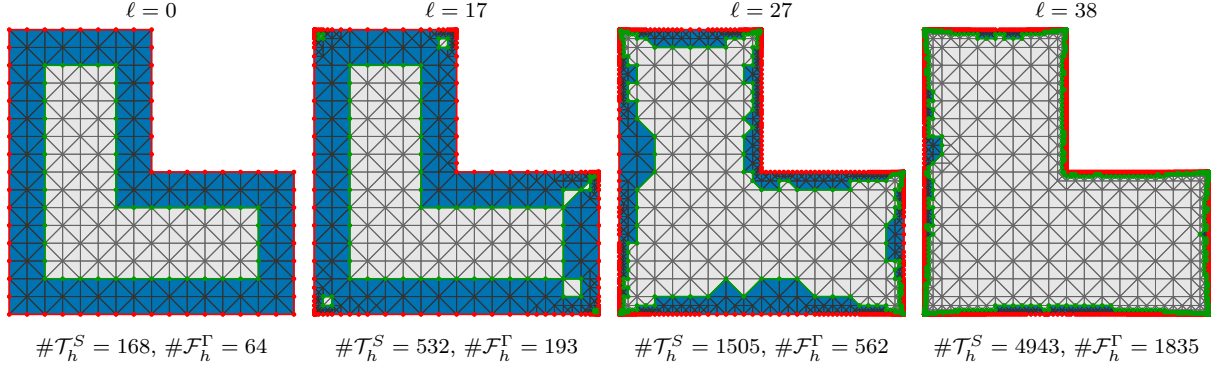


FIGURE 5. Adaptively generated meshes in Example 5.2 for $p = 1$ and $\theta = 0.6$; see Figure 2 for the color code.

Here, the potential error $\|\nabla(u - u_h)\|_{L^2(\Omega)} \approx \|\nabla I_h(u - u_h)\|_{L^2(\Omega)}$ is computed by numerical quadrature. More precisely, we employ the \mathcal{P}^2 -nodal interpolant $I_h : C(\bar{\Omega}) \rightarrow \mathcal{S}^2(\mathcal{T}_h^{\text{unif}})$ on a (three times) uniform refinement $\mathcal{T}_h^{\text{unif}}$ of the finest adaptive mesh \mathcal{T}_h . We stress that the plot neglects the non-accessible constant C_{osc} from (20). The results for $p = 1$ and $p = 2$ are similar. For uniform mesh-refinement, we obtain the expected reduced order of convergence. For adaptive mesh-refinement, we regain the optimal order of convergence. Moreover, for adaptive mesh-refinement, we see that the majorant is, in fact, a sharp estimate for the (in general unknown) potential error. The computed minorant is less accurate. However, we stress that the minorant is always computed on the same boundary layer as the majorant (which is obtained by adaptivity driven by the majorant). The empirical values for uniform (resp. adaptive) mesh-refinement are also provided in Table 1 (resp. Table 2). The accuracy of the lower bound could be improved by appropriately adapting a second boundary layer (not displayed). Figure 4 compares the numerical results for different choices of the adaptivity parameter $\theta \in \{0.2, 0.4, 0.6, 0.8\}$. We observe that any choice of θ regains, in fact, the optimal convergence rate.

Example 5.2 (Smooth potential in L-shaped domain). We consider problem (1) with prescribed exact solution

$$u(x) = \cosh(x_1) \cos(x_2) \quad \text{for all } x \in \Omega := (0, 1/2)^2 \setminus ([1/4, 1/2] \times [0, 1/4]) \quad (27)$$

on the L-shaped domain Ω with diameter $\text{diam}(\Omega) = \sqrt{1/2}$. We start Algorithm 9 with an initial triangulation \mathcal{T}_h of Ω into $\#T_0 = 384$ right triangles.

As in Section 5.1, the potential u is smooth, but the sought density ϕ of the indirect BEM formulation lacks regularity. The initial meshes as well as some adaptively generated meshes are visualized in Figure 5. Figure 6 visualizes some numerical results for uniform and adaptive mesh-refinement, where we proceed as in Section 5.1. Since $p = 1$ and $p = 2$ lead to similar results (not displayed), we only report the results for $p = 1$.

As expected from theory, the shape of Ω does not impact the functional error estimates: Overall, the results obtained correspond to those from Section 5.1, where uniform mesh-refinement leads to a suboptimal convergence behavior, which is cured by means of the proposed adaptive strategy.

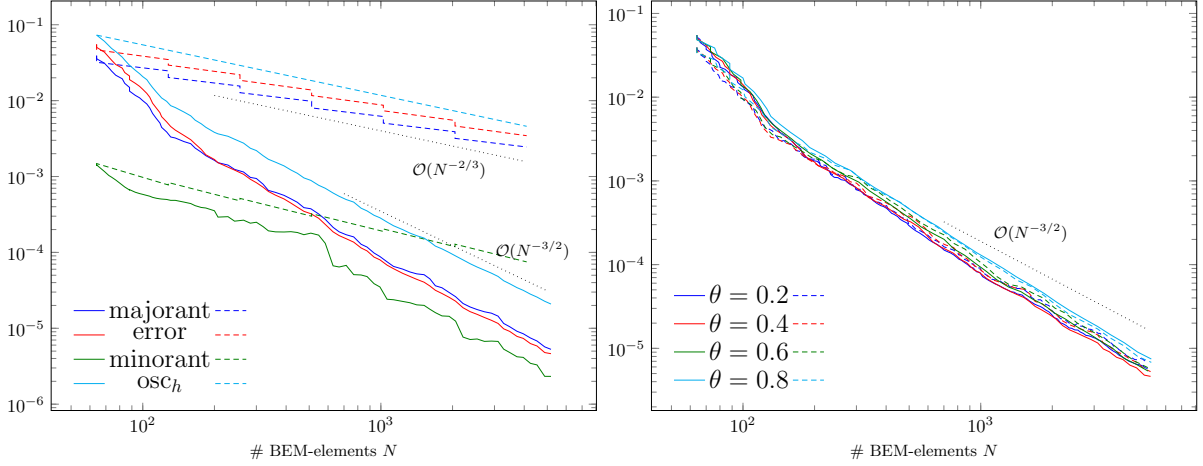


FIGURE 6. Comparison of adaptive vs. uniform mesh-refinement in Example 5.2. The majorant is computed by \mathcal{P}^1 -FEM. *Left:* We compare the potential error $\|\nabla(u - u_h)\|_{L^2(\Omega)}$, the majorant $\|\nabla w_h\|_{L^2(\Omega)}$ from (16), the data oscillations osc_h from (20), and the minorant $\mathfrak{M}(\tau_h)^{1/2}$ from (25) for uniform (dashed) and adaptive mesh-refinement (solid) with $\theta = 0.4$. *Right:* We compare the potential error (solid) and the majorant (dashed) for adaptive mesh-refinement for various choices of θ .

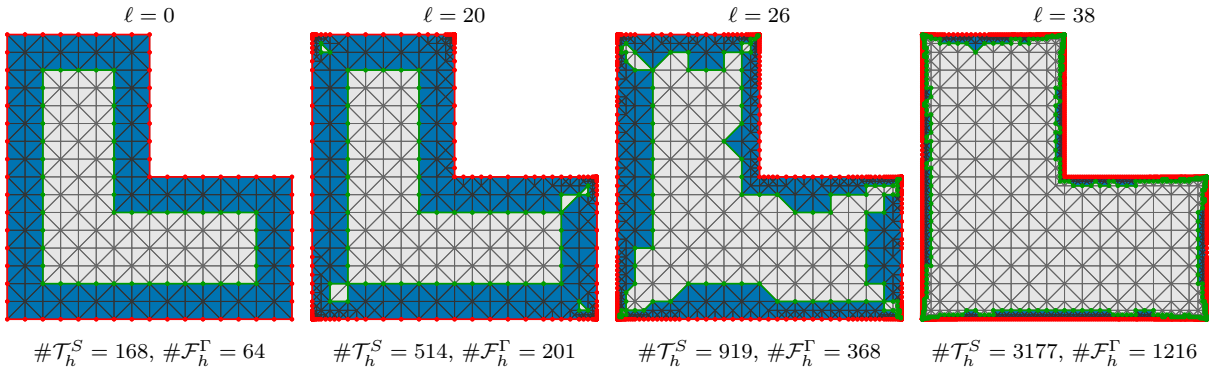


FIGURE 7. Adaptively generated meshes in Example 5.3 for $p = 1$ and $\theta = 0.6$; see Figure 2 for the color code.

Example 5.3 (Non-smooth potential in L-shaped domain). We consider problem (1) with prescribed exact solution

$$u(x) = r^{2/3} \cos(2\varphi/3) \quad \text{for all } x \in \Omega := (0, 1/2)^2 \setminus [(1/4, 1/2] \times [0, 1/4]] \quad (28)$$

given in standard polar coordinates $x = x(r, \varphi)$ on the L-shaped domain Ω with diameter $\text{diam}(\Omega) = \sqrt{1/2}$. We start Algorithm 9 with an initial triangulation \mathcal{T}_0 of Ω into $\#\mathcal{T}_0 = 384$ right triangles.

Unlike Section 5.1 and Section 5.2, the potential u is non-smooth at $(0, 0)$. The initial meshes as well as some adaptively generated meshes are visualized in Figure 7. Numerical

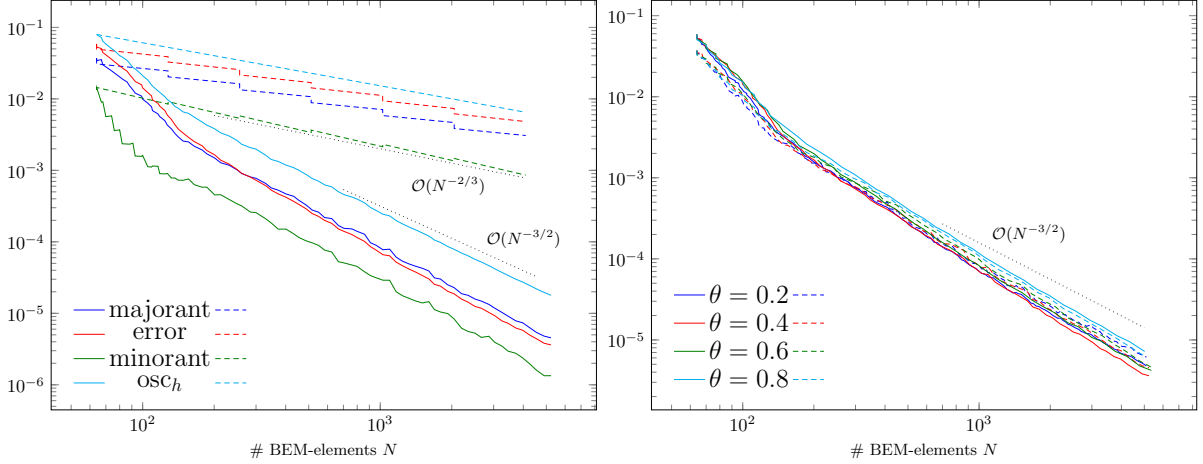


FIGURE 8. Comparison of adaptive vs. uniform mesh-refinement in Example 5.3. The majorant is computed by \mathcal{P}^1 -FEM. *Left:* We compare the potential error $\|\nabla(u - u_h)\|_{L^2(\Omega)}$, the majorant $\|\nabla w_h\|_{L^2(\Omega)}$ from (16), the data oscillations osc_h from (20), and the minorant $\mathfrak{M}(\tau_h)^{1/2}$ from (25) for uniform (dashed) and adaptive mesh-refinement (solid) with $\theta = 0.4$. *Right:* We compare the potential error (solid) and the majorant (dashed) for adaptive mesh-refinement for various choices of θ .

convergence results are visualized in Figure 8. Moreover, Table 3 provides some empirical values for adaptive mesh-refinement. Our observations are the same as in Section 5.1 and Section 5.2 and underline that the functional error bounds do not rely on any *a priori* smoothness of the unknown potential u : While uniform mesh-refinement leads to a suboptimal convergence behavior, the proposed adaptive strategy regains the optimal convergence rate.

6. EXTENSION OF THE ANALYSIS

So far, we have considered functional *a posteriori* error estimation for an indirect BEM formulation (10) discretized by Galerkin BEM (11). The following sections address some obvious extensions of our analysis. While the subsequent numerical experiments (as well as those from Section 5) focus on $d = 2$, we again stress that the theoretical results also apply to arbitrary dimensions, in particular to $d = 3$. However, 3D experiments are beyond the scope of this work and left to future research.

6.1. Collocation BEM. It is worth noting that all results of Section 3 hold, in particular, for any $v = \tilde{V}\phi_h$ with arbitrary $\phi_h \in \mathbf{H}^{-1/2}(\Gamma)$. Consequently, the computable bounds of Theorem 4 (resp. Corollary 5) hold for any approximation $\phi_h \approx \phi$. In particular, Algorithm 9 can also be applied to (e.g., lowest-order) collocation BEM, where $\phi_h \in \mathcal{P}^0(\mathcal{F}_h^\Gamma)$ is determined by collocation conditions

$$(V\phi_h)(x_F) = g(x_F) \quad \text{for all } F \in \mathcal{F}_h^\Gamma, \quad (29)$$

ℓ	$\#\mathcal{F}_h^\Gamma$	$\frac{\#\mathcal{T}_h^S}{\#\mathcal{F}_h^\Gamma}$	$\text{dof}(\mathcal{T}_h^S)$	$\ \nabla(u - u_h)\ _{L^2(\Omega)}$	$\ \nabla w_h\ _{L^2(S)}$	$\frac{\ \nabla w_h\ _{L^2(S)}}{\ \nabla(u - u_h)\ _{L^2(\Omega)}}$	$\frac{\ \nabla w_h\ _{L^2(S)}}{\mathfrak{M}(\tau_h)^{1/2}}$
0	64	2.63	33	$5.87e - 2$	$3.72e - 2$	0.64	2.79
6	76	2.57	39	$3.32e - 2$	$2.30e - 2$	0.69	6.41
12	93	2.62	46	$1.75e - 2$	$1.21e - 2$	0.69	7.60
18	116	2.60	81	$8.65e - 3$	$6.16e - 3$	0.71	5.40
24	141	2.68	132	$3.80e - 3$	$2.95e - 3$	0.78	4.04
30	201	2.68	215	$1.65e - 3$	$1.49e - 3$	0.90	3.28
36	300	2.65	336	$7.26e - 4$	$7.74e - 4$	1.07	3.02
42	454	2.59	491	$3.34e - 4$	$3.82e - 4$	1.14	3.31
48	667	2.62	715	$1.51e - 4$	$1.69e - 4$	1.12	3.21
54	961	2.60	1023	$7.66e - 5$	$8.95e - 5$	1.17	2.85
60	1412	2.56	1447	$3.76e - 5$	$4.55e - 5$	1.21	3.06
66	2042	2.57	2048	$1.88e - 5$	$2.30e - 5$	1.22	2.73
72	3031	2.53	2927	$9.28e - 6$	$1.18e - 5$	1.27	3.00
78	4548	2.51	4283	$4.40e - 6$	$4.80e - 6$	1.23	3.38
80	5232	2.49	4835	$3.61e - 6$	$4.54e - 6$	1.26	3.39

TABLE 3. Adaptive mesh-refinement with $\theta = 0.4$ in Example 5.3. We focus on the degrees of freedom, the potential error $\|\nabla(u - u_h)\|_{L^2(\Omega)}$, the accuracy of the \mathcal{P}^1 -FEM majorant $\|\nabla w_h\|_{L^2(\Omega)}$ from (16), and the width of the confidence interval given by the quotient of majorant and minorant.

where $x_F \in F$ is an appropriate collocation node (e.g., the center of mass). We stress that well-posedness of collocation BEM is non-obvious (see, e.g., [CPS92, CPS93, MP96]). However, this does not affect our developed functional *a posteriori* error bounds.

6.2. Other BEM ansatz spaces. With the same argument as for collocation BEM, one can replace the discrete BEM ansatz space $\mathcal{P}^0(\mathcal{F}_h^\Gamma) \ni \phi_h$ by an arbitrary discrete space $\mathcal{P}_h \subseteq \mathbf{H}^{-1/2}(\Gamma)$ (e.g., higher-order piecewise polynomials, splines, isogeometric NURBS, etc.). For $r \in \mathbb{N}_0$ and $\mathcal{P}_h = \mathcal{P}^r(\mathcal{F}_h^\Gamma)$, we expect that the choices $p = r + 1$ and $q = r$ will lead to accurate computable upper and lower bounds in Theorem 4. The numerical validation of this expectation is, however, beyond the scope of the present work.

6.3. Direct BEM approach. The indirect BEM approach makes ansatz (10) for the unknown solution of (9). Unlike this, the direct BEM approach is based on the Green's third identity: Any solution of (9) can be written as the sum of a single-layer and a double-layer potential, i.e.,

$$u(x) = [\tilde{V}\phi](x) - [\tilde{K}g](x) := [\tilde{V}\phi](x) - \int_{\Gamma} \partial_{\mathbf{n}(y)} G(x - y) g(y) \, dy \quad \text{for all } x \in \Omega, \quad (30)$$

where $g = u|_{\Gamma} \in \mathbf{H}^{1/2}(\Gamma)$ is the trace of u (i.e., the Dirichlet data) and $\phi = \mathbf{n} \cdot \nabla u|_{\Gamma} \in \mathbf{H}^{-1/2}(\Gamma)$ is the normal derivative (i.e., the Neumann data). Taking the trace of this identity and respecting the jump properties of the double-layer potential (see,

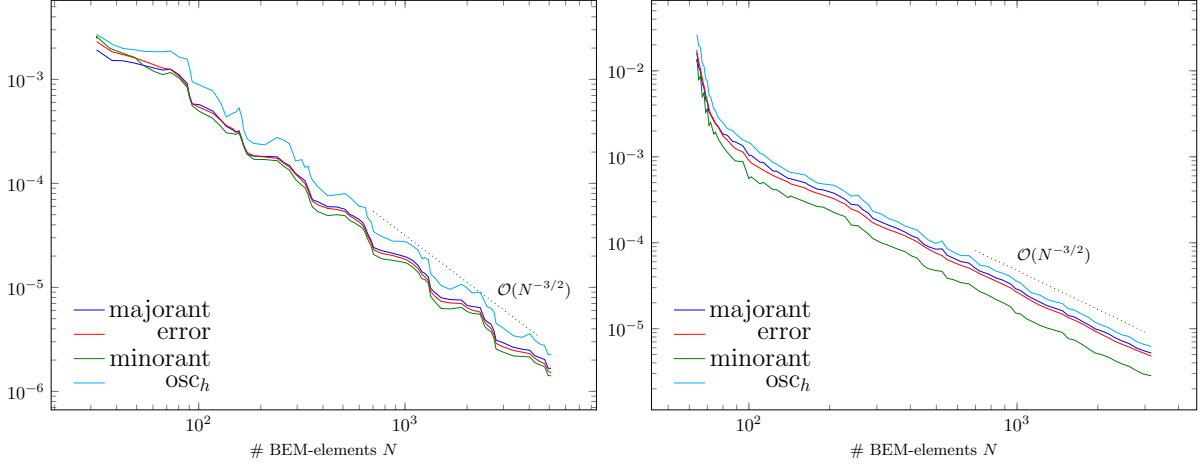


FIGURE 9. Numerical results for adaptive mesh-refinement ($\theta = 0.4$) in Example 6.4 (left) and Example 6.5 (right). We plot the potential error $\|\nabla(u - u_h)\|_{L^2(\Omega)}$, the majorant $\|\nabla w_h\|_{L^2(\Omega)}$ from (16) based on \mathcal{P}^1 -FEM, the data oscillations osc_h from (34), and the minorant $\underline{\mathfrak{M}}(\tau_h)^{1/2}$ from (25).

ℓ	$\#\mathcal{F}_h^\Gamma$	$\frac{\#\mathcal{T}_h^S}{\#\mathcal{F}_h^\Gamma}$	$\text{dof}(\mathcal{T}_h^S)$	$\ \nabla(u - u_h)\ _{L^2(\Omega)}$	$\ \nabla w_h\ _{L^2(S)}$	$\frac{\ \nabla w_h\ _{L^2(S)}}{\ \nabla(u - u_h)\ _{L^2(\Omega)}}$	$\frac{\ \nabla w_h\ _{L^2(S)}}{\underline{\mathfrak{M}}(\tau_h)^{1/2}}$
0	32	2.25	15	$2.30e-3$	$1.92e-3$	0.83	0.78
5	49	2.61	54	$1.61e-3$	$1.43e-3$	0.89	0.88
11	88	2.76	110	$8.68e-4$	$9.12e-4$	1.05	1.09
17	147	2.79	161	$3.61e-4$	$3.53e-4$	0.98	1.15
23	172	2.76	203	$1.98e-4$	$1.90e-4$	0.96	1.00
29	295	2.93	387	$1.23e-4$	$1.25e-4$	1.02	1.15
35	377	2.85	442	$6.23e-5$	$6.68e-5$	1.07	1.24
41	599	2.89	743	$4.25e-5$	$4.50e-5$	1.06	1.15
47	770	2.88	901	$2.12e-5$	$2.26e-5$	1.06	1.20
53	1210	2.93	1533	$1.33e-5$	$1.40e-5$	1.06	1.16
59	1652	2.96	2005	$7.09e-6$	$7.64e-6$	1.08	1.23
65	2500	2.99	3228	$4.36e-6$	$4.69e-6$	1.08	1.18
71	3696	2.91	4988	$2.38e-6$	$2.55e-6$	1.07	1.18
77	5099	2.99	6483	$1.50e-6$	$1.66e-6$	1.11	1.18

TABLE 4. Adaptive mesh-refinement with $\theta = 0.4$ in Example 6.4. We focus on the degrees of freedom, the potential error $\|\nabla(u - u_h)\|_{L^2(\Omega)}$, the accuracy of the \mathcal{P}^1 -FEM majorant $\|\nabla w_h\|_{L^2(\Omega)}$ from (16), and the width of the confidence interval given by the quotient of majorant and minorant.

e.g., [McL00, Ste08a, HW08, SS11, GS18]), one sees that

$$g = V\phi - (K - 1/2)g \quad \text{in } H^{1/2}(\Gamma),$$

ℓ	$\#\mathcal{F}_h^\Gamma$	$\frac{\#\mathcal{T}_h^S}{\#\mathcal{F}_h^\Gamma}$	$\text{dof}(\mathcal{T}_h^S)$	$\ \nabla(u - u_h)\ _{L^2(\Omega)}$	$\ \nabla w_h\ _{L^2(S)}$	$\frac{\ \nabla w_h\ _{L^2(S)}}{\ \nabla(u - u_h)\ _{L^2(\Omega)}}$	$\frac{\ \nabla w_h\ _{L^2(S)}}{\mathfrak{M}(\tau_h)^{1/2}}$
0	64	2.63	33	$1.74e - 2$	$1.61e - 2$	0.93	0.74
6	69	2.62	37	$5.30e - 3$	$4.64e - 3$	0.88	0.80
12	77	2.69	42	$2.20e - 3$	$2.22e - 3$	1.01	0.95
18	100	2.57	46	$9.06e - 4$	$1.04e - 3$	1.15	1.21
24	140	2.50	79	$5.07e - 4$	$5.60e - 4$	1.10	1.16
30	208	2.58	159	$3.25e - 4$	$3.76e - 4$	1.16	1.16
36	279	2.61	248	$1.88e - 4$	$2.21e - 4$	1.18	1.20
42	404	2.59	381	$1.10e - 4$	$1.20e - 4$	1.09	1.19
48	549	2.62	531	$6.35e - 5$	$7.14e - 5$	1.12	1.30
54	780	2.67	790	$3.93e - 5$	$4.33e - 5$	1.10	1.23
60	1085	2.67	1131	$2.28e - 5$	$2.46e - 5$	1.08	1.33
66	1550	2.73	1695	$1.35e - 5$	$1.42e - 5$	1.05	1.29
72	2203	2.71	2372	$7.78e - 6$	$7.92e - 6$	1.02	1.32
78	3166	2.74	3442	$4.80e - 6$	$5.20e - 6$	1.08	1.29

TABLE 5. Adaptive mesh-refinement with $\theta = 0.4$ in Example 6.5. We focus on the degrees of freedom, the potential error $\|\nabla(u - u_h)\|_{L^2(\Omega)}$, the accuracy of the \mathcal{P}^1 -FEM majorant $\|\nabla w_h\|_{L^2(\Omega)}$ from (16), and the width of the confidence interval given by the quotient of majorant and minorant.

where K formally coincides with \tilde{K} , but is evaluated for $x \in \Gamma$ instead. Elementary calculations then lead to the variational formulation

$$\langle V\phi, \psi \rangle_\Gamma = \langle (K + 1/2)g, \psi \rangle_\Gamma \quad \text{for all } \psi \in \mathbf{H}^{-1/2}(\Gamma). \quad (31)$$

We stress that the factor $1/2$ is only valid almost everywhere on Γ and hence correct for the variational formulation and Galerkin BEM, while collocation BEM would require a modification at corners (and additionally along edges in 3D); see [McL00, Ste08a, HW08].

Usual implementations approximate $g \approx g_h \in \mathcal{S}^p(\mathcal{F}_h^\Gamma)$ so that the integral operators in (31) are only evaluated for discrete functions. Overall, the lowest-order Galerkin BEM formulation then reads

$$\langle V\phi_h, \psi_h \rangle_{L^2(\Gamma)} = \langle (K + 1/2)g_h, \psi_h \rangle_{L^2(\Gamma)} \quad \text{for all } \psi_h \in \mathcal{P}^0(\mathcal{F}_h^\Gamma). \quad (32)$$

As above, the Lax–Milgram lemma proves that (31) (resp. (32)) admit unique solutions $\phi \in \mathbf{H}^{-1/2}(\Gamma)$ (resp. $\phi_h \in \mathcal{P}^0(\mathcal{F}_h^\Gamma)$). Moreover, the computed density ϕ_h is now indeed an approximation of the Neumann data $\mathbf{n} \cdot \nabla u|_\Gamma = \partial_{\mathbf{n}} u|_\Gamma = \phi \approx \phi_h$. Defining

$$u_h(x) = [\tilde{V}\phi_h](x) - [\tilde{K}g_h](x) \quad \text{for } x \in \Omega, \quad (33)$$

one obtains an approximation u_h of the solution $u = \tilde{V}\phi - \tilde{K}g$ of (9) (resp. (30)). We stress that $u_h|_\Gamma = V\phi_h + (1/2 - K)g_h$ so that the data oscillation term in the upper bound

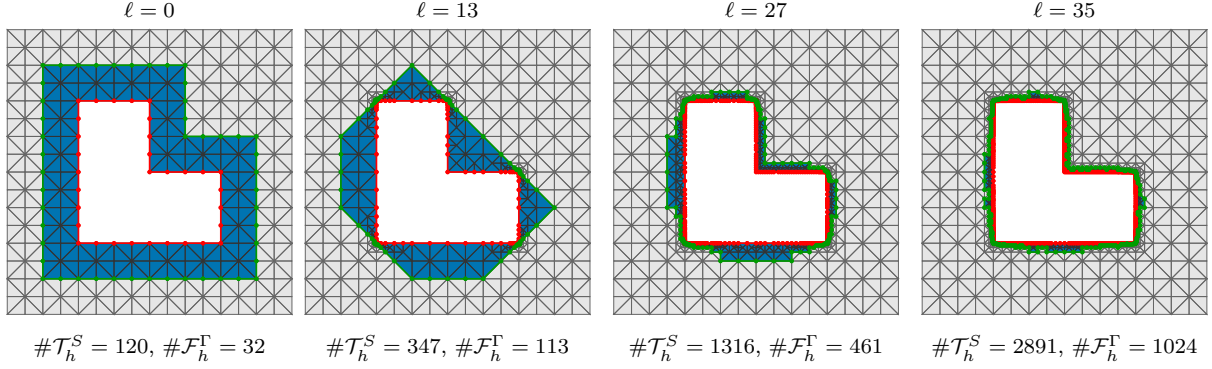


FIGURE 10. Adaptively generated meshes ($\theta = 0.6$) in Example 6.7. We indicate the boundary layer \mathbf{S} (blue), the boundary $\mathbf{\Gamma}$ (red), and the interior boundary $\mathbf{\Gamma}^c = \partial\mathbf{S} \setminus \mathbf{\Gamma}$ (green); see Figure 2 for the color code.

of Theorem 4 reads

$$\begin{aligned}
\|\nabla(u - u_h)\|_{L^2(\Omega)} &\leq \min_{\substack{w \in H^1(\Omega) \\ w|_\Gamma = J_h(g - u_h)|_\Gamma}} \|\nabla w\|_{L^2(\Omega)} + \|(1 - J_h)(g - V\phi_h - (1/2 - K)g_h)\|_{H^{1/2}(\Gamma)} \\
&\leq \min_{\substack{w \in H^1(\Omega) \\ w|_\Gamma = J_h(g - u_h)|_\Gamma}} \|\nabla w\|_{L^2(\Omega)} + C_{\text{osc}}^2 \text{osc}_h,
\end{aligned} \tag{34a}$$

where $J_h : L^2(\Gamma) \rightarrow \mathcal{S}^1(\mathcal{F}_h^\Gamma)$ is the $L^2(\Gamma)$ -orthogonal projection and

$$\text{osc}_h := \|h^{1/2} \nabla_\Gamma [(1 - J_h)(g - V\phi_h - (1/2 - K)g_h)]\|_{L^2(\Gamma)}; \tag{34b}$$

see Section 4.2. In our implementation, we also employed $g_h = J_h g \in \mathcal{S}^1(\mathcal{F}_h^\Gamma)$.

Example 6.4 (Direct BEM for smooth potential in square domain). We consider the setting (26) from Section 5.1. Applying the direct BEM approach (31), we know that $\phi_h \approx \phi = \mathbf{n} \cdot \nabla u|_\Gamma$, where ϕ (as well as the potential u) is smooth. In this particular situation, we know that uniform mesh-refinement would already lead to the optimal convergence behavior (not displayed). The same is empirically observed for the proposed adaptive strategy, where we even observe that the majorant $\|\nabla w_h\|_{L^2(\Omega)}$ from (16) as well as the minorant $\mathfrak{M}(\tau_h)^{1/2}$ from (25) provide sharp error bounds for the potential error $\|\nabla(u - u_h)\|_{L^2(\Omega)}$; see Figure 9 (left) as well as Table 4.

Example 6.5 (Direct BEM for non-smooth potential in L-shaped domain). We consider the setting (28) from Section 5.3. Applying the direct BEM approach (31), we know that $\phi_h \approx \phi = \mathbf{n} \cdot \nabla u|_\Gamma$, where ϕ (as well as the potential u) is only non-smooth with a singularity at $(0,0)$. Also for this case, the proposed adaptive strategy regains the optimal convergence rate; see Figure 9 (right) as well as Table 5. Even though the quotient $\|\nabla w_h\|_{L^2(\Omega)} / \mathfrak{M}(\tau_h)^{1/2}$ of the computable upper and lower bound is larger than for the smooth problem of Section 6.4, we observe that the lower bound is, in fact, much more accurate for the direct BEM than for the indirect BEM computations from Section 5.

6.6. Unbounded domains. One particular strength of BEM is that it naturally

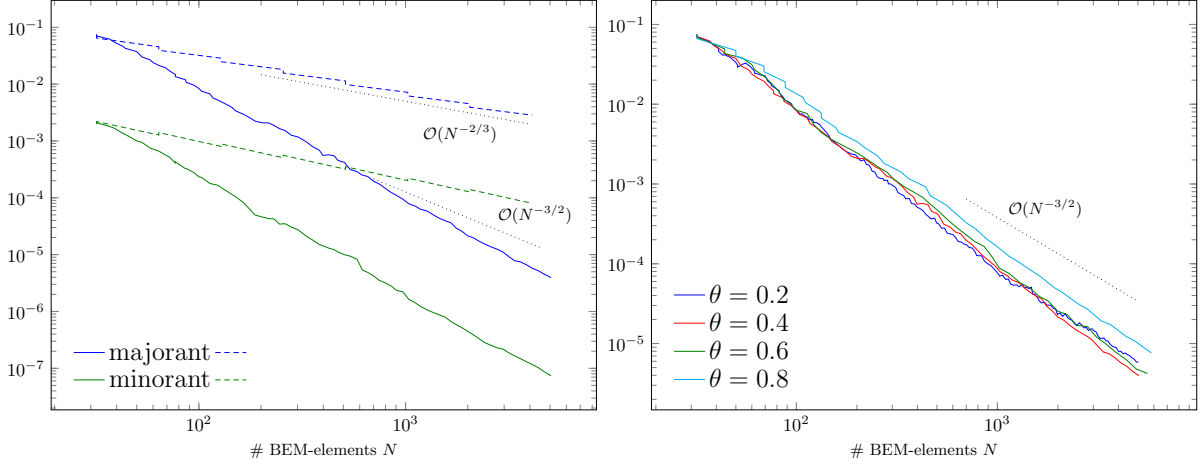


FIGURE 11. Comparison of adaptive vs. uniform mesh-refinement in Example 6.7. The majorant is computed by \mathcal{P}^1 -FEM. *Left:* Since the potential error $\|\nabla(u - u_h)\|_{L^2(\Omega)}$ is unknown and $\text{osc}_h = 0$, we only compare the majorant $\|\nabla w_h\|_{L^2(\Omega)}$ from (16) and the minorant $\mathfrak{M}(\tau_h)^{1/2}$ from (25) for uniform (dashed) and adaptive mesh-refinement (solid) with $\theta = 0.4$. *Right:* We compare the majorant for adaptive mesh-refinement for various choices of θ .

allows to consider also exterior domain problems formulated on unbounded Lipschitz domains $\Omega^c := \mathbb{R}^d \setminus \overline{\Omega}$. In this case, the homogeneous Dirichlet–Laplace problem subject to given inhomogeneous boundary data g reads

$$\Delta u = 0 \quad \text{in } \Omega^c, \quad u = g \quad \text{on } \Gamma, \quad (35a)$$

supplemented by the radiation (decay) condition (for $|x| \rightarrow \infty$)

$$u(x) = \mathcal{O}(\log |x|) \quad \text{for } d = 2 \quad \text{resp.} \quad u(x) = \mathcal{O}(1/|x|) \quad \text{for } d = 3. \quad (35b)$$

We note that the latter radiation condition is naturally incorporated into the potential operators (due to the choice of the fundamental solution with right decay) arising in BEM, e.g., any single-layer potential $\tilde{V}\phi_h$ satisfies (35b).

We note that the functional error identity from Theorem 3 (with Ω being replaced by the exterior domain Ω^c) remains valid (in principal) for any $v \in \mathbf{L}_{\text{loc}}^2(\Omega^c)$ with $\nabla v \in \mathbf{L}^2(\Omega^c)$ and $\Delta v = 0$. Consequently, the computable upper and lower bounds of Theorem 4 (resp. Corollary 5) hold (with appropriate modifications) for any approximation $\phi_h \approx \phi$ and $v := \tilde{V}\phi_h$. In particular, Algorithm 9 can also be applied to BEM for exterior domain problems.

Example 6.7 (Direct BEM for exterior problem). To illustrate the latter observation, we consider the exterior domain

$$\Omega^c := \mathbb{R}^2 \setminus \overline{\Omega}, \quad \Omega = (0, 1/2)^2 \setminus \left([(1/4, 1/2] \times [0, 1/4] \right),$$

where Ω is the L-shaped domain from Section 5.2. We consider (35) with constant Dirichlet data

$$g = 1 = (1/2 - K)1 \quad \text{on } \Gamma, \quad (36)$$

where K is the double-layer integral operator. Consequently, the corresponding indirect BEM formulation (10) turns out to be a direct BEM formulation for the exterior domain problem [McL00, SS11], where all data oscillation terms vanish. Thus, one can expect that the sought density $\phi \in H^{-1/2}(\Gamma)$ has singularities at the convex corners of Ω (but *not* at the reentrant corner).

We employ Algorithm 9 (with Galerkin BEM). The initial mesh \mathcal{T}_h with $\#\mathcal{T}_h = 416$ right triangles is a triangulation of $(-1/4, 3/4)^2 \setminus \overline{\Omega} \subset \Omega^c$; see Figure 10. Some numerical results are shown in Figure 11. Since the exact potential u is unknown, we cannot compute the potential error $\|\nabla(u - u_h)\|_{L^2(\Omega)}$. However, adaptive mesh-refinement leads to the optimal convergence behavior of majorant and minorant (and hence also of $\|\nabla(u - u_h)\|_{L^2(\Omega)}$).

7. CONCLUSION

We have presented, for the first time, functional error estimates for BEM. Not only that the presented estimates are independent of the specific discretization method (i.e., Galerkin or collocation), they also provide guaranteed upper and lower bounds for the unknown energy error. This is in contrast to existing techniques, which usually contain generic constants. The error bounds are obtained by solving auxiliary variational problems by a finite element method on a strip. In the paper, we consider the Dirichlet problem of the Laplace equation, but the approach is expected to generalize to other boundary value problems. In the considered case, the upper error bound is based on the Dirichlet principle, while the lower error bound is based either on a variational problem in terms of a potential (scalar stream function in 2D and vector potential in 3D) or a mixed problem (in 2D and 3D). The upper bound is localized and drives an adaptive refinement of the boundary mesh. Since the finite element strip contains always two layers of elements, it geometrically shrinks towards the boundary during refinement. This way, the ratio between the degrees of freedom (DoF) for obtaining the error estimates and the BEM DoF remains bounded. We have examined various 2D test problems on square and L-shaped domains, with and without singular potential, including exterior problems. The proposed adaptive algorithm exhibited excellent performance. In all cases, the optimal convergence rates could be achieved.

Suggested further research work concerns an implementation of the algorithm in 3D and the extension to electromagnetic scattering problems.

APPENDIX A. SOME REMARKS ON THE ANALYSIS

We recall the notations introduced in Section 2.1, in particular, the harmonic extension operator $\widehat{(\cdot)} : H^{1/2}(\Gamma) \rightarrow H^1(\Omega)$ from (6). Moreover, we add the definitions of

$$\begin{aligned} H_{\Gamma^c}^1(S) &:= \overline{\{\varphi|_S : \varphi \in C^\infty(\mathbb{R}^d), \text{supp } \varphi \text{ compact, } \text{dist}(\text{supp } \varphi, \Gamma^c) > 0\}}^{H^1(S)} \\ &= \{\varphi \in H^1(S) : \varphi|_{\Gamma^c} = 0\}, \end{aligned}$$

see, e.g., [BPS16], for the density result, and

$$\mathbf{H}_{\Gamma^c}(\operatorname{div}, S) := \overline{\{\boldsymbol{\sigma}|_S : \boldsymbol{\sigma} \in \mathbf{C}^\infty(\mathbb{R}^d), \operatorname{supp} \boldsymbol{\sigma} \text{ compact}, \operatorname{dist}(\operatorname{supp} \boldsymbol{\sigma}, \Gamma^c) > 0\}}^{\mathbf{H}(\operatorname{div}, S)}.$$

The latter space generalizes the (partial) homogeneous boundary condition $\mathbf{n} \cdot \boldsymbol{\sigma}|_{\Gamma^c} = 0$ to functions $\boldsymbol{\sigma} \in \mathbf{H}(\operatorname{div}, S)$. Note that the natural trace $\mathbf{n} \cdot \boldsymbol{\sigma}|_{\partial S}$ can be 'restricted' to, e.g., Γ in the following sense.

Remark 11. *Functions in $\mathbf{H}_{\Gamma^c}^1(S)$ vanish at Γ^c . In particular, any function $\varphi \in \mathbf{H}_{\Gamma^c}^1(S)$ can be extended by zero to a function $\varphi \in \mathbf{H}^1(\Omega)$. Analogously, vector fields in $\mathbf{H}_{\Gamma^c}(\operatorname{div}, S)$ have vanishing normal component at Γ^c in a weak sense. In particular, any vector field $\boldsymbol{\sigma} \in \mathbf{H}_{\Gamma^c}(\operatorname{div}, S)$ can be extended by zero to a vector field $\boldsymbol{\sigma} \in \mathbf{H}(\operatorname{div}, \Omega)$. Hence, the normal trace $\mathbf{n} \cdot \boldsymbol{\sigma}|_{\partial S} \in \mathbf{H}^{-1/2}(\partial S)$ of $\boldsymbol{\sigma}$ may be identified with a well defined element $\mathbf{n} \cdot \boldsymbol{\sigma}|_\Gamma \in \mathbf{H}^{-1/2}(\Gamma)$ vanishing on Γ^c in a weak sense.*

Let us discuss the minimiser $\bar{w} = u - v$ of the upper bound and the maximiser $\underline{\boldsymbol{\tau}} = \nabla \bar{w}$ of the lower bound from Theorem 3 in more detail. Note that¹

$$\begin{aligned} \bar{w} &= u - v \in \mathbf{H}^1(\Omega), & \underline{\boldsymbol{\tau}} &= \nabla \bar{w} \in \mathbf{H}(\operatorname{div}, \Omega) \cap \mathbf{H}(\operatorname{curl}, \Omega), \\ \Delta \bar{w} &= 0 \text{ in } \Omega, & \operatorname{div} \underline{\boldsymbol{\tau}} &= 0 \text{ in } \Omega, \\ & & \operatorname{curl} \underline{\boldsymbol{\tau}} &= 0 \text{ in } \Omega, \\ \bar{w}|_\Gamma &= g - v|_\Gamma \text{ on } \Gamma, & \mathbf{n} \times \underline{\boldsymbol{\tau}}|_\Gamma &= \nabla_\Gamma(g - v|_\Gamma) \text{ in } \mathbf{H}^{-1/2}(\Gamma). \end{aligned} \tag{37}$$

Moreover, by replacing w with $\bar{w} + \varepsilon \varphi$ and by replacing $\boldsymbol{\tau}$ with $\underline{\boldsymbol{\tau}} + \varepsilon \boldsymbol{\sigma}$ in (12), where $\varphi \in \mathbf{H}_0^1(\Omega)$ and $\boldsymbol{\sigma} \in \mathbf{H}(\operatorname{div}, \Omega)$ with $\operatorname{div} \boldsymbol{\sigma} = 0$ as well as $\varepsilon \in \mathbb{R}$, we obtain the variational formulations

$$\forall \varphi \in \mathbf{H}_0^1(\Omega) \quad \langle \nabla \bar{w}, \nabla \varphi \rangle_{\mathbf{L}^2(\Omega)} = 0, \tag{38a}$$

$$\forall \boldsymbol{\sigma} \in \mathbf{H}(\operatorname{div}, \Omega) \text{ with } \operatorname{div} \boldsymbol{\sigma} = 0 \quad \langle \underline{\boldsymbol{\tau}}, \boldsymbol{\sigma} \rangle_{\mathbf{L}^2(\Omega)} = \langle g - v|_\Gamma, \mathbf{n} \cdot \boldsymbol{\sigma}|_\Gamma \rangle_\Gamma. \tag{38b}$$

Let $\psi \in \mathbf{H}^{1/2}(\Gamma)$ and let $\widehat{\psi} \in \mathbf{H}^1(\Omega)$ be its harmonic extension. Testing the second variational formulation (38b) with $\boldsymbol{\sigma} = \nabla \widehat{\psi}$ shows

$$\langle \psi, \mathbf{n} \cdot \underline{\boldsymbol{\tau}}|_\Gamma \rangle_\Gamma = \langle g - v|_\Gamma, \mathbf{n} \cdot \nabla \widehat{\psi}|_\Gamma \rangle_\Gamma.$$

Thus, additionally to the scalar and tangential boundary conditions for \bar{w} and $\underline{\boldsymbol{\tau}}$ in (37), respectively, we have also found a normal boundary condition for $\underline{\boldsymbol{\tau}} = \nabla \bar{w}$, namely

$$\mathbf{n} \cdot \underline{\boldsymbol{\tau}}|_\Gamma = \langle g - v|_\Gamma, \mathbf{n} \cdot \nabla(\widehat{\cdot})|_\Gamma \rangle_\Gamma \quad \text{in } \mathbf{H}^{-1/2}(\Gamma). \tag{39}$$

This shows that there are different options for computing \bar{w} and $\underline{\boldsymbol{\tau}}$.

Remark 12. *Note that*

$$\partial_n(\widehat{\cdot})|_\Gamma = \mathbf{n} \cdot \nabla(\widehat{\cdot})|_\Gamma : \mathbf{H}^{1/2}(\Gamma) \rightarrow \mathbf{H}^{-1/2}(\Gamma)$$

¹As the exterior derivative commutes with the trace operator, which is simply the pull-back of the canonical embedding of the boundary manifold Γ into $\overline{\Omega}$ (i.e., $\iota^* \mathrm{d} = \mathrm{d}\iota^*$), we see for the special case of $\varphi \in \mathbf{H}^1(\Omega)$ that $\mathbf{n} \times \nabla \varphi|_\Gamma = \nabla_\Gamma \varphi|_\Gamma$ in $\mathbf{H}^{-1/2}(\Gamma)$, where $\mathbf{n} \times (\cdot)|_\Gamma : \mathbf{H}(\operatorname{curl}, \Omega) \rightarrow \mathbf{H}^{-1/2}(\Gamma)$ denotes the tangential trace and $\nabla_\Gamma : \mathbf{H}^{1/2}(\Gamma) \rightarrow \mathbf{H}^{-1/2}(\Gamma)$ the surface gradient.

is the well known Dirichlet-to-Neumann operator for the homogeneous Laplacian. Moreover, the normal trace of $\underline{\tau}$ in (39) does not depend on the harmonic extension as

$$\langle g - v|_{\Gamma}, \mathbf{n} \cdot \nabla \widehat{\psi}|_{\Gamma} \rangle_{\Gamma} = \langle \psi, \mathbf{n} \cdot \underline{\tau}|_{\Gamma} \rangle_{\Gamma} = \langle \psi, \mathbf{n} \cdot \nabla(u - v)|_{\Gamma} \rangle_{\Gamma} \quad \text{for all } \psi \in H^{1/2}(\Gamma).$$

Recalling Theorem 3 and Theorem 4, we note the following.

Remark 13 (Minimiser of the upper bound). *The unique minimiser \bar{w} of the upper bound is the unique harmonic extension of $g - v|_{\Gamma}$ to Ω , i.e., $\bar{w} \in H^1(\Omega)$ is the unique solution of the Dirichlet–Laplace problem*

$$\Delta \bar{w} = 0 \text{ in } \Omega, \quad \bar{w}|_{\Gamma} = g - v|_{\Gamma} \text{ on } \Gamma.$$

It holds $\langle \nabla \bar{w}, \nabla \varphi \rangle_{L^2(\Omega)} = 0$ for all $\varphi \in H_0^1(\Omega)$. Moreover, $\bar{w} \in H^1(\Omega)$ solves the Neumann Laplace problem

$$\Delta \bar{w} = 0 \text{ in } \Omega, \quad \mathbf{n} \cdot \nabla \bar{w}|_{\Gamma} = \langle g - v|_{\Gamma}, \mathbf{n} \cdot \nabla(\widehat{\cdot})|_{\Gamma} \rangle_{\Gamma} \quad \text{in } H^{-1/2}(\Gamma).$$

It holds $\langle \nabla \bar{w}, \nabla \varphi \rangle_{L^2(\Omega)} = \langle g - v|_{\Gamma}, \mathbf{n} \cdot \nabla(\widehat{\varphi}|_{\Gamma})|_{\Gamma} \rangle_{\Gamma}$ for all $\varphi \in H^1(\Omega)$. Note that, at least analytically, both formulations can also be used to find the unique maximiser $\underline{\tau} = \nabla \bar{w}$ of the upper bound. For numerical purposes the Dirichlet–Laplace problem is the better and easier choice to compute \bar{w} .

Next we want to find equations and variational formulations for $\underline{\tau}$ not involving \bar{w} . For this, let us introduce Dirichlet and Neumann fields

$$\begin{aligned} \mathcal{H}_D(\Omega) &:= \{ \boldsymbol{\sigma} \in H_0(\text{curl}, \Omega) \cap H(\text{div}, \Omega) : \text{curl } \boldsymbol{\sigma} = 0, \text{div } \boldsymbol{\sigma} = 0 \}, \\ \mathcal{H}_N(\Omega) &:= \{ \boldsymbol{\sigma} \in H(\text{curl}, \Omega) \cap H_0(\text{div}, \Omega) : \text{curl } \boldsymbol{\sigma} = 0, \text{div } \boldsymbol{\sigma} = 0 \}, \end{aligned}$$

where

$$\begin{aligned} H_0(\text{curl}, \Omega) &:= \overline{\{ \boldsymbol{\sigma} \in C^\infty(\Omega) : \text{supp } \boldsymbol{\sigma} \text{ compact in } \Omega \}}^{H(\text{curl}, \Omega)}, \\ H_0(\text{div}, \Omega) &:= \overline{\{ \boldsymbol{\sigma} \in C^\infty(\Omega) : \text{supp } \boldsymbol{\sigma} \text{ compact in } \Omega \}}^{H(\text{div}, \Omega)}. \end{aligned}$$

We compute

$$\begin{aligned} \forall \boldsymbol{\sigma} \in \mathcal{H}_D(\Omega) \quad & \langle \underline{\tau}, \boldsymbol{\sigma} \rangle_{L^2(\Omega)} = \langle g - v|_{\Gamma}, \mathbf{n} \cdot \boldsymbol{\sigma}|_{\Gamma} \rangle_{\Gamma}, \\ \forall \boldsymbol{\sigma} \in \mathcal{H}_N(\Omega) \quad & \langle \underline{\tau}, \boldsymbol{\sigma} \rangle_{L^2(\Omega)} = 0. \end{aligned}$$

Remark 14 (Maximiser of the lower bound). *The unique maximiser $\underline{\tau} = \nabla \bar{w}$ of the lower bound is the unique solution of the electro-static Maxwell problem*

$$\begin{aligned} \text{curl } \underline{\tau} &= 0 & \text{in } \Omega, \\ \text{div } \underline{\tau} &= 0 & \text{in } \Omega, \\ \mathbf{n} \times \underline{\tau}|_{\Gamma} &= \nabla_{\Gamma}(g - v|_{\Gamma}) & \text{in } H^{-1/2}(\Gamma), \\ \langle \underline{\tau}, \boldsymbol{\sigma} \rangle_{L^2(\Omega)} &= \langle g - v|_{\Gamma}, \mathbf{n} \cdot \boldsymbol{\sigma}|_{\Gamma} \rangle_{\Gamma} & \text{for all } \boldsymbol{\sigma} \in \mathcal{H}_D(\Omega), \end{aligned}$$

as well as the unique solution of the magneto-static Maxwell problem

$$\begin{aligned} \operatorname{curl} \underline{\tau} &= 0 & \text{in } \Omega, \\ \operatorname{div} \underline{\tau} &= 0 & \text{in } \Omega, \\ \mathbf{n} \cdot \underline{\tau}|_{\Gamma} &= \langle g - v|_{\Gamma}, \mathbf{n} \cdot \nabla(\cdot)|_{\Gamma} \rangle_{\Gamma} & \text{in } H^{-1/2}(\Gamma), \\ \langle \underline{\tau}, \sigma \rangle_{L^2(\Omega)} &= 0 & \text{for all } \sigma \in \mathcal{H}_N(\Omega). \end{aligned}$$

See [Pic81, Pic82, Pau19, BPS16] for proper solution theories.

As $\underline{\tau} \in H(\operatorname{div}, \Omega)$ with $\operatorname{div} \underline{\tau} = 0$, by (38b) the vector field $\underline{\tau}$ solves for all $\omega \in L^2(\Omega)$ the mixed problem

$$\begin{aligned} \langle \underline{\tau}, \sigma \rangle_{L^2(\Omega)} + \langle \operatorname{div} \sigma, \omega \rangle_{L^2(\Omega)} &= \langle g - v|_{\Gamma}, \mathbf{n} \cdot \sigma|_{\Gamma} \rangle_{\Gamma}, \\ \langle \operatorname{div} \underline{\tau}, \psi \rangle_{L^2(\Omega)} &= 0 \end{aligned}$$

for all $(\sigma, \psi) \in H(\operatorname{div}, \Omega) \times L^2(\Omega)$ with $\operatorname{div} \sigma = 0$. On the other hand, especially for numerical reasons, we want to skip the solenoidal conditions, which leads to the following mixed variational saddle point formulation (cf. Theorem 4).

Lemma 15 (Mixed problem for the lower bound). *Let $v \in H^1(\Omega)$ with $\Delta v = 0$. Then the mixed problem*

$$\begin{aligned} \langle \tau, \sigma \rangle_{L^2(\Omega)} + \langle \operatorname{div} \sigma, \omega \rangle_{L^2(\Omega)} &= \langle g - v|_{\Gamma}, \mathbf{n} \cdot \sigma|_{\Gamma} \rangle_{\Gamma}, \\ \langle \operatorname{div} \tau, \psi \rangle_{L^2(\Omega)} &= 0 \end{aligned}$$

for all $(\sigma, \psi) \in H(\operatorname{div}, \Omega) \times L^2(\Omega)$, admits a unique solution $(\tau, \omega) \in H(\operatorname{div}, \Omega) \times L^2(\Omega)$. Moreover, $(\tau, \omega) = (\underline{\tau}, \bar{w})$, i.e., the latter mixed formulation can be used to compute the unique maximiser $\underline{\tau} = \nabla \bar{w}$ and the unique minimiser \bar{w} simultaneously.

Remark 16. *The mixed formulation in Lemma 15 is the mixed formulation of the Dirichlet–Laplace problem from Remark 13. For numerical purposes the latter mixed formulation is only a good choice to compute $\underline{\tau}$, since the numerical approximations will only satisfy $(\tau, \omega) \in H(\operatorname{div}, \Omega) \times L^2(\Omega)$ but in general not $\omega \in H^1(\Omega)$.*

Proof of Lemma 15. The inner product $\langle \cdot, \cdot \rangle_{L^2(\Omega)}$ is positive on the kernel $\{\sigma \in H(\operatorname{div}, \Omega) : \operatorname{div} \sigma = 0\}$ and the inf-sup-condition is satisfied as for $\psi \in L^2(\Omega)$

$$\sup_{\sigma \in H(\operatorname{div}, \Omega)} \frac{\langle \operatorname{div} \sigma, \psi \rangle_{L^2(\Omega)}}{\|\sigma\|_{H(\operatorname{div}, \Omega)} \|\psi\|_{L^2(\Omega)}} \geq \frac{\|\psi\|_{L^2(\Omega)}}{\sqrt{\|\sigma_{\psi}\|_{L^2(\Omega)}^2 + \|\psi\|_{L^2(\Omega)}^2}} \geq \frac{1}{\sqrt{c_F^2 + 1}}.$$

This follows by solving a Dirichlet–Laplace problem, i.e., by finding the unique solution $\omega_{\psi} \in H_0^1(\Omega)$ of

$$\Delta \omega_{\psi} = \psi \text{ in } \Omega, \quad \omega_{\psi}|_{\Gamma} = 0 \text{ on } \Gamma,$$

and setting $\sigma_{\psi} = \nabla \omega_{\psi}$. Note that the estimate $\|\sigma_{\psi}\|_{L^2(\Omega)} \leq c_F \|\psi\|_{L^2(\Omega)}$ holds true, where $0 < c_F \leq \operatorname{diam}(\Omega)/\pi$ is the Friedrichs constant for the gradient operator on $H_0^1(\Omega)$. Therefore, the standard saddle point theory for mixed problems shows the unique solvability, see, e.g., [BBF13]. Moreover, we have $\operatorname{div} \tau = 0$ by the second line of the mixed formulation. Testing the first line with compactly supported test vector fields σ

shows that $\omega \in H^1(\Omega)$ with $\nabla \omega = \boldsymbol{\tau}$. Hence $\Delta \omega = \operatorname{div} \boldsymbol{\tau} = 0$. Furthermore, the first line implies

$$\langle \omega|_{\Gamma}, \mathbf{n} \cdot \boldsymbol{\sigma}|_{\Gamma} \rangle_{\Gamma} = \langle g - v|_{\Gamma}, \mathbf{n} \cdot \boldsymbol{\sigma}|_{\Gamma} \rangle_{\Gamma}$$

for all $\boldsymbol{\sigma} \in \mathbf{H}(\operatorname{div}, \Omega)$, yielding $\omega|_{\Gamma} = g - v|_{\Gamma}$ by the surjectivity of the normal trace operator $\mathbf{n} \cdot (\cdot)|_{\Gamma}$. Thus $\omega = u - v = \bar{w}$ and $\boldsymbol{\tau} = \nabla \omega = \nabla \bar{w} = \underline{\boldsymbol{\tau}}$. \square

Remark 17. *The continuous version of (17) in Corollary 5 reads: Find $w \in H_{\Gamma^c}^1(S)$ such that*

$$\langle \nabla w, \nabla \varphi \rangle_{L^2(S)} = \langle g - v|_{\Gamma}, \mathbf{n} \cdot \operatorname{curl} \varphi|_{\Gamma} \rangle_{\Gamma} \quad \text{for all } \varphi \in H_{\Gamma^c}^1(S). \quad (40)$$

Then $w \in H^1(S)$ is the unique solution of the mixed Dirichlet–Neumann–Laplace problem

$$\Delta w = 0 \text{ in } S, \quad w|_{\Gamma^c} = 0 \text{ on } \Gamma^c, \quad \mathbf{n} \cdot \nabla w|_{\Gamma} = \langle g - v|_{\Gamma}, \mathbf{n} \cdot \operatorname{curl} (\widehat{\cdot})_{\partial S}|_{\Gamma} \rangle_{\Gamma} \text{ in } H^{-1/2}(\Gamma).$$

To see this, we pick different test functions. Testing (40) with compactly supported (in S) smooth functions shows $\Delta w = 0$ in S , and by definition, i.e., $w \in H_{\Gamma^c}^1(S)$, it is clear that $w|_{\Gamma^c} = 0$ on Γ^c . Let $\phi \in H^{1/2}(\Gamma)$, define

$$\phi_{\partial S} := \begin{cases} \phi & \text{on } \Gamma, \\ 0 & \text{on } \Gamma^c, \end{cases}$$

and let $\varphi := \widehat{\phi_{\partial S}} \in H^1(S)$ be the unique harmonic extension to S of $\phi_{\partial S}$, compare to (6). Then $\varphi \in H_{\Gamma^c}^1(S)$ and testing (40) with φ yields

$$\langle g - v|_{\Gamma}, \mathbf{n} \cdot \operatorname{curl} \widehat{\phi_{\partial S}}|_{\Gamma} \rangle_{\Gamma} = \langle \phi, \mathbf{n} \cdot \nabla w|_{\Gamma} \rangle_{\Gamma},$$

i.e., $\mathbf{n} \cdot \nabla w|_{\Gamma} = \langle g - v|_{\Gamma}, \mathbf{n} \cdot \operatorname{curl} (\widehat{\cdot})_{\partial S}|_{\Gamma} \rangle_{\Gamma}$ in $H^{-1/2}(\Gamma)$.

By construction, \tilde{w} , the extension by zero to Ω , belongs to $H^1(\Omega)$ and hence we have $\boldsymbol{\tau} := \operatorname{curl} \tilde{w} \in \mathbf{H}(\operatorname{div}, \Omega)$ with $\operatorname{div} \boldsymbol{\tau} = 0$. Theorem 3 shows

$$2 \langle g - v|_{\Gamma}, \mathbf{n} \cdot \operatorname{curl} \tilde{w}|_{\Gamma} \rangle_{\Gamma} - \|\nabla w\|_{L^2(S)}^2 \leq \|\nabla(u - v)\|_{L^2(\Omega)}^2.$$

REFERENCES

- [AEF⁺14] Markus Aurada, Michael Ebner, Michael Feischl, Samuel Ferraz-Leite, Thomas Führer, Petra Goldenits, Michael Karkulik, Markus Mayr, and Dirk Praetorius. HILBERT—a MATLAB implementation of adaptive 2D-BEM. *Numer. Algorithms*, 67(1):1–32, 2014.
- [AFF⁺15] Markus Aurada, Michael Feischl, Thomas Führer, Michael Karkulik, and Dirk Praetorius. Energy norm based error estimators for adaptive BEM for hypersingular integral equations. *Appl. Numer. Math.*, 95:15–35, 2015.
- [AFK⁺13] Markus Aurada, Michael Feischl, Josef F. Kemetmüller, Marcus Page, and Dirk Praetorius. Each $H^{1/2}$ -stable projection yields convergence and quasi-optimality of adaptive FEM with inhomogeneous Dirichlet data in \mathbb{R}^d . *ESAIM Math. Model. Numer. Anal.*, 47(4):1207–1235, 2013.
- [AP19] Immanuel Anjam and Dirk Pauly. An elementary method of deriving a posteriori error equalities and estimates for linear partial differential equations. *Comput. Methods Appl. Math.*, 19(2):311–322, 2019.
- [BBF13] Daniele Boffi, Franco Brezzi, and Michel Fortin. *Mixed finite element methods and applications*. Springer, Heidelberg, 2013.

- [BC05] Corinna Bahriawati and Carsten Carstensen. Three MATLAB implementations of the lowest-order Raviart-Thomas MFEM with a posteriori error control. *Comput. Methods Appl. Math.*, 5(4):333–361, 2005.
- [BCD04] Sören Bartels, Carsten Carstensen, and Georg Dolzmann. Inhomogeneous Dirichlet conditions in a priori and a posteriori finite element error analysis. *Numer. Math.*, 99(1):1–24, 2004.
- [BPS16] Sebastian Bauer, Dirk Pauly, and Michael Schomburg. The Maxwell compactness property in bounded weak Lipschitz domains with mixed boundary conditions. *SIAM J. Math. Anal.*, 48(4):2912–2943, 2016.
- [Car97] Carsten Carstensen. An a posteriori error estimate for a first-kind integral equation. *Math. Comp.*, 66(217):139–155, 1997.
- [CF01] Carsten Carstensen and Birgit Faermann. Mathematical foundation of a posteriori error estimates and adaptive mesh-refining algorithms for boundary integral equations of the first kind. *Eng. Anal. Bound. Elem.*, 25(7):497 – 509, 2001.
- [CMS01] Carsten Carstensen, Matthias Maischak, and Ernst P. Stephan. A posteriori error estimate and h -adaptive algorithm on surfaces for Symm’s integral equation. *Numer. Math.*, 90(2):197–213, 2001.
- [CPS92] Martin Costabel, Frank Penzel, and Reinhold Schneider. Error analysis of a boundary element collocation method for a screen problem in \mathbf{R}^3 . *Math. Comp.*, 58(198):575–586, 1992.
- [CPS93] Martin Costabel, Frank Penzel, and Reinhold Schneider. Convergence of boundary element collocation methods for Dirichlet and Neumann screen problems in \mathbf{R}^3 . *Appl. Anal.*, 49(1-2):101–117, 1993.
- [CS95] Carsten Carstensen and Ernst P. Stephan. A posteriori error estimates for boundary element methods. *Math. Comp.*, 64(210):483–500, 1995.
- [CT87] Michel Crouzeix and Vidar Thomée. The stability in L_p and W_p^1 of the L_2 -projection onto finite element function spaces. *Math. Comp.*, 48(178):521–532, 1987.
- [EH06] Vincent J. Ervin and Norbert Heuer. An adaptive boundary element method for the exterior Stokes problem in three dimensions. *IMA J. Numer. Anal.*, 26(2):297–325, 2006.
- [FFH⁺15] Michael Feischl, Thomas Führer, Norbert Heuer, Michael Karkulik, and Dirk Praetorius. Adaptive boundary element methods. *Arch. Comput. Methods Eng.*, 22(3):309–389, 2015.
- [FFK⁺14] Michael Feischl, Thomas Führer, Michael Karkulik, Jens Markus Melenk, and Dirk Praetorius. Quasi-optimal convergence rates for adaptive boundary element methods with data approximation, part I: weakly-singular integral equation. *Calcolo*, 51(4):531–562, 2014.
- [FFP19] Thomas Führer, Stefan Funken, and Dirk Praetorius. Adaptive isoparametric P2-FEM: Analysis and efficient MATLAB implementation. *in preparation*, 2019.
- [FLP08] Samuel Ferraz-Leite and Dirk Praetorius. Simple a posteriori error estimators for the h -version of the boundary element method. *Computing*, 83(4):135–162, 2008.
- [FPP14] Michael Feischl, Marcus Page, and Dirk Praetorius. Convergence and quasi-optimality of adaptive FEM with inhomogeneous Dirichlet data. *J. Comput. Appl. Math.*, 255:481–501, 2014.
- [FPW11] Stefan Funken, Dirk Praetorius, and Philipp Wissgott. Efficient implementation of adaptive P1-FEM in Matlab. *Comput. Methods Appl. Math.*, 11(4):460–490, 2011.
- [GHS16] Fernando D. Gaspoz, Claus-Justus Heine, and Kunibert G. Siebert. Optimal grading of the newest vertex bisection and H^1 -stability of the L_2 -projection. *IMA J. Numer. Anal.*, 36(3):1217–1241, 2016.
- [GS18] Joachim Gwinner and Ernst P. Stephan. *Advanced boundary element methods*. Springer, Cham, 2018.
- [HW08] George C. Hsiao and Wolfgang L. Wendland. *Boundary integral equations*. Springer, Berlin, 2008.
- [KPP13] Michael Karkulik, David Pavlicek, and Dirk Praetorius. On 2D newest vertex bisection: optimality of mesh-closure and H^1 -stability of L_2 -projection. *Constr. Approx.*, 38(2):213–234, 2013.
- [McL00] William McLean. *Strongly elliptic systems and boundary integral equations*. Cambridge University Press, Cambridge, 2000.

- [MP96] William McLean and Siegfried B. Prökdorf. Boundary element collocation methods using splines with multiple knots. *Numer. Math.*, 74(4):419–451, 1996.
- [MSW98] Patrick Mund, Ernst P. Stephan, and Joscha Weiße. Two-level methods for the single layer potential in \mathbf{R}^3 . *Computing*, 60(3):243–266, 1998.
- [Pau19] Dirk Pauly. Solution theory, variational formulations, and functional a posteriori error estimates for general first order systems with applications to electro-magneto-statics and more. *Numer. Funct. Anal. Optim.*, 2019.
- [Pic81] Rainer Picard. Randwertaufgaben der verallgemeinerten Potentialtheorie. *Math. Methods Appl. Sci.*, 3:218–228, 1981.
- [Pic82] Rainer Picard. On the boundary value problems of electro- and magnetostatics. *Proc. Roy. Soc. Edinburgh Sect. A*, 92:165–174, 1982.
- [Rep00] Sergey I. Repin. A posteriori error estimation for variational problems with uniformly convex functionals. *Math. Comp.*, 69(230):481–500, 2000.
- [Rep08] Sergey I. Repin. *A posteriori estimates for partial differential equations*. De Gruyter, Berlin, 2008.
- [Seb19] Daniel Sebastian. *Functional a posteriori error estimates for boundary element methods*. Master thesis, Universität Duisburg Essen, 2019.
- [SS11] Stefan A. Sauter and Christoph Schwab. *Boundary element methods*. Springer, Berlin, 2011.
- [Ste08a] Olaf Steinbach. *Numerical approximation methods for elliptic boundary value problems*. Springer, New York, 2008.
- [Ste08b] Rob Stevenson. The completion of locally refined simplicial partitions created by bisection. *Math. Comp.*, 77(261):227–241, 2008.
- [SV06] Roberta Sacchi and Andreas Veiser. Locally efficient and reliable a posteriori error estimators for Dirichlet problems. *Math. Models Methods Appl. Sci.*, 16(3):319–346, 2006.

TU WIEN, INSTITUTE FOR ANALYSIS AND SCIENTIFIC COMPUTING, WIEDNER HAUPTSTRASSE 8-10/E101/4, 1040 VIENNA, AUSTRIA

E-mail address: `dirk.praetorius@asc.tuwien.ac.at` (corresponding author)

E-mail address: `daniel.sebastian@asc.tuwien.ac.at`

TU DARMSTADT, CENTRE FOR COMPUTATIONAL ENGINEERING, DOLIVOSTRASSE 15, 64293 DARMSTADT, GERMANY

E-mail address: `kurz@gsc.tu-darmstadt.de`

UNIVERSITÄT DUISBURG-ESSEN, FAKULTÄT FÜR MATHEMATIK, THEA-LEYMANN-STRASSE 9, 45141 ESSEN, GERMANY

E-mail address: `dirk.pauly@uni-due.de`

UNIVERSITY OF JYVÄSKYLÄ, BUILDING AGORA, MATILANNIEMI 2, 40100 JYVÄSKYLÄ, FINLAND

RUSSIAN ACADEMY OF SCIENCES, STEKLOV INSTITUTE OF MATHEMATICS, 191011, FONTANKA 27, ST. PETERSBURG, RUSSIA

E-mail address: `sergey.repin@mit.jyu.fi`

E-mail address: `repin@pdmi.ras.ru`